On retrieving the microphysical properties of cirrus clouds using the moments of the millimeter-wavelength Doppler spectrum

Gerald G. Mace
Department of Meteorology, University of Utah, Salt Lake City, Utah, USA

Andrew J. Heymsfield
National Center for Atmospheric Research, Boulder, Colorado, USA

Michael R. Poellot
Department of Atmospheric Sciences, University of North Dakota, Grand Forks, North Dakota, USA

Received 19 September 2001; revised 26 March 2002; accepted 15 April 2002; published 31 December 2002.

[1] Techniques that use only measurements provided by millimeter-wavelength Doppler radar for retrieving the properties of clouds provide certain practical advantages over techniques that require measurements from multiple instruments. We concentrate on the capacity of the moments of the Doppler spectrum to provide information suitable for retrieving the microphysical properties of cirrus clouds. Specifically, we present an algorithm that uses the zeroth and first moments of the Doppler spectrum (radar reflectivity and mean Doppler velocity) to retrieve the cloud particle size distribution. We also discuss a methodology for evaluating the second moment of the Doppler spectrum for information related to the width of the particle size distribution. The properties of observed cirrus particle spectra are first examined to ascertain what degree of complexity is required of assumed functional representations of particle spectra in cirrus volumes. We find that although particle spectra with bimodal tendencies are common, single-mode functions are able to capture the essential characteristics of these spectra to within observational uncertainty for most cirrus. Furthermore, two-parameter functions such as the exponential function are shown to be adequate representations of cirrus particle spectra in situations where the radar reflectivity factor is less than about -5 dBZ_e and the temperatures are colder than about 253 K. A technique for separating air motion contributions from the Doppler velocity is examined, and an approach for similarly processing the Doppler spectral width is introduced. In comparison to aircraft data, we find uncertainty in the derived quiet air velocity and spectrum width to be on the order of 20% and 40%, respectively. Using recent parameterizations of ice crystal terminal velocity, mass, and backscatter cross section, we present a straightforward algorithm for retrieving cirrus cloud microphysical properties from observations of radar reflectivity and Doppler velocity. A simulation experiment with variable particle habits and realistic observational error shows that the retrieval uncertainties are on the order of 60% and 40% for ice water content and mass median particle size, respectively. These uncertainty magnitudes are supported by comparison to aircraft data. *INDEX TERMS:* 3394 Meteorology and Atmospheric Dynamics: Instruments and techniques; 3360 Meteorology and Atmospheric Dynamics: Remote sensing; 0320 Atmospheric Composition and Structure: Cloud physics and chemistry; 0394 Atmospheric Composition and Structure: Instruments and techniques; *KEYWORDS:* cirrus clouds, cloud property retrievals, millimeter radar, Doppler radar, cirrus microphysical properties

Citation: Mace, G. G., A. J. Heymsfield, and M. R. Poellot, On retrieving the microphysical properties of cirrus clouds using the moments of the millimeter-wavelength Doppler spectrum, *J. Geophys. Res.*, *107*(D24), 4815, doi:10.1029/2001JD001308, 2002.

1. Introduction

[2] Ice phase clouds of the upper troposphere are a component of the hydrologic cycle that in a mass-weighted sense exert an enormous influence on the Earth's energy budget. The general characteristics of these clouds range from the barely visible but ubiquitous cirrus near the tropical tropopause [*McFarquhar et al.*, 2000] to optically thick cloud systems associated with frontal systems, jet streams and deep convective outflows. (While cirrus are strictly defined as optically thin ice-phase clouds of the upper

0148-0227/02/2001JD001308

troposphere, for convenience we expand that definition in this paper to include all upper tropospheric clouds whose composition is primarily ice regardless of their optical thickness.) Upper tropospheric clouds have been linked to phenomena as diverse as the dehydration of the stratosphere [*Jensen et al.*, 1996] and to thermal regulation of the global tropics [*Ramanathan and Collins*, 1991]. The overall importance of cirrus to the global climate system has also been demonstrated with numerical models. *Lohmann and Roeckner* [1995], for instance, demonstrates that the climate of a general circulation model (GCM) is quite sensitive to the microphysical characteristics of upper tropospheric clouds. Other studies have found similar sensitivities [e.g., *Stephens et al.*, 1990] and have shown that under some circumstances cirrus can exert either a cooling or warming effect on the atmospheric column [*Ackerman et al.*, 1988].

[3] While our knowledge of the characteristics of cirrus has improved significantly in recent years due to long-term observational programs [*Sassen et al.*, 2001] and several field programs [e.g., *Starr*, 1987; *Rashke*, 1988] as well as a concerted modeling effort on the part a few researchers [*Sassen and Dodd*, 1988; *Starr and Cox*, 1985; *Heymsfield and Sabin*, 1989], a good deal remains to be learned. In particular, our demonstrated ability to accurately parameterize cirrus in GCMs has not improved significantly since the seminal studies of *Heymsfield and Platt* [1984]. While many attempts have been made to develop new parameterizations of cirrus optical properties [*Platt and Harshvardan*, 1988; *Ebert and Curry*, 1992; *Fu and Liou*, 1993], our understanding of the coupling between the macroscale and microphysical cirrus cloud properties with the large-scale atmosphere (i.e., that which can be resolved by GCMs) remains fundamentally deficient. Due primarily to a lack of observations, the few physically based parameterizations of cirrus properties that have emerged [e.g., *Heymsfield and Donner*, 1990] suffer from a lack of verification. Indeed our general ability to accurately characterize cirrus cloud properties in terms of the large-scale atmospheric state represent one of the milestones that must be achieved before predictions of global climate change with numerical models can have credibility.

[4] There are several avenues toward reaching the goal of improved cloud parameterization in general and cirrus parameterization in particular. *Randall et al.* [1996] outline several possible approaches ranging from the use of single column GCMs to the use of high-resolution cloud resolving models. A common necessary theme in each of these strategies, however, is a sufficient observational database with which to validate model output. While the use of global satellite-derived observational data such as ISCCP [*Rossow and Schiffer*, 1999] will always be important in this regard, a complimentary observational database of broad scope is being generated by the Atmospheric Radiation Measurement program (ARM; *Stokes and Schwartz* [1994]) at four sites using suites of operational surface-based remote sensors. The instrument compliments at these sites range from all manner of radiometry including broadband hemispheric measurements and narrowband spectrometers to operational lidars such as the micropulse lidar system (MPL; *Spinhirne* [1993]) and millimeter cloud radars (MMCR; *Moran et al.* [1998]). The MMCRs represents the centerpiece of the cloud observing instrument suite. Coupled with ceilometers and the MPLs the MMCR data provide as complete a description of the vertical time series of hydrometer occurrence as has ever been recorded at single locations. Since the installation of the first MMCR at the Southern Great Plains (SGP) site in Oklahoma in late 1996, MMCRs have been installed at the north slope of Alaska site (NSA) near Barrow and at the tropical Pacific (TWP) site near Nauru in mid 1998. An MMCR was installed at the Manus Island TWP site in June 1999.

[5] The operational ARM data are routinely calibrated, cloud masked, and multiple data streams are merged to form a continuous record of hydrometeor occurrence above the ARM sites [*Clothiaux et al.*, 2000]. This record has a temporal resolution of better than 1 minute and vertical resolution of at least 90m throughout the vertical column. This record of hydrometeor occurrence contributes to understanding an important component of the cloud parameterization problem by documenting the vertical distribution and occurrence frequency of hydrometeors over these sites. Several researchers have begun to use this information to validate cloud occurrence in atmospheric models [*Mace et al.*, 1998a] and to investigate the cloud overlap problem [*Hogan and Illingworth*, 2000; *Mace and Benson-Troth*, 2002]. Ultimately, this record will be combined with large-scale meteorological analyses to investigate the actual relationships between cloud layer occurrence and the scale of motion that can be resolved by GCMs. While documenting the occurrence of hydrometeors is obviously important, knowledge of the cloud microphysical properties is also required to understand how the layers interact with the radiation streams and influence the water and heat budgets in vertical columns above the sites.

[6] While observations of cloud occurrence are derived directly from the active and passive sensor datastreams, cloud microphysical properties must be derived with algorithms that use some combination of theoretical understanding, empirical knowledge and reasonable assumptions to convert some number of observations into geophysical parameters of interest. The simplest form of retrieval algorithms emerged from early work by D. Atlas and others in the middle 1950s and early 1960s [*Atlas*, 1954, 1964; *Atlas and Bartnoff*, 1953] in the form of straightforward regression equations applied to radar reflectivity observations in order to derive rain rate. The regression approach to cloud property retrieval remains applicable today [*Liu and Illingworth*, 2000], although the uncertainty of results derived from such approaches has been shown to be substantial [*Atlas et al.*, 1995]. Retrieval algorithms evolved by combining multiple data streams to estimate the properties of various classes of clouds such as cirrus [*Platt*, 1979; *Platt et al.*, 1998] and boundary layer clouds [*Frisch et al.*, 1995]. Since the early 1990s, S. Matrosov and collaborators at the NOAA Environmental Technology Laboratory have developed a hierarchy of algorithms [*Matrosov et al.*, 1992, 1994] that rely on combining millimeter radar data with thermal radiance observations [see also *Matrosov et al.*, 1996, 1999, 2000]. *Mace et al.* [1998b] adapted the technique described by *Matrosov et al.* [1992] and applied it to the continuous MMCR and infrared spectrometer data streams collected at the SGP site. More recently, microphysical properties from extended time periods have been analyzed [*Mace et al.*, 2001; *Wang and Sassen*, 2002].

[7] Most nonregression-based cirrus property retrieval algorithms designed for application to surface-based data are derived with a similar set of assumptions and have had similar limitations. The Matrosov set of algorithms, for instance, and those derived from them [*Mace et al.*, 1998b] use some combination of millimeter wave Doppler radar data and another observation related to a vertical integral of the ice mass such as downwelling infrared radiance. This information is used to derive the parameters of a particle size distribution of specified functional form. These algorithms assume that the size distribution conforms to unimodal first order gamma or modified gamma functions. While this class of algorithm has been shown to be reasonably accurate (30% uncertainty for mean particle size and 50% uncertainty in ice water content [*Matrosov et al.*, 1994]), they have limitations and many of the basic assumptions in their derivation have been accepted without much question. For instance, it is necessary that the infrared radiometer has a clear line of sight to the cloud layer (no clouds can exist below the cirrus) and the cirrus layer must be optically thin. (If we assume a precision in retrieving the layer emissivity of 10%, then one can show that this equates to an uncertainty in absorption optical depth of approximately 1.75 and, assuming 0.5 for the single scattering albedo, to an extinction optical depth of about 3.5.) Using a continuous year of data collected at the SGP site *Mace et al.* [2001] show these conditions are violated as much as 30% of the time. *Mace et al.* [1997] found lower layers blocking upper tropospheric clouds nearly 40% of the time using data collected during autumn in the northeastern United States. Initial analysis of data collected at the NSA and the TWP sites show that boundary layer clouds are predominant. When cirrus clouds are observed, they occur simultaneously with lower level clouds much of the time.

[8] Certain assumptions about the size distribution also contribute to a residual uncertainty in retrieval algorithms. The use of gamma functions in cirrus clouds follows from the seminal study of *Kosarev and Mazin* [1991] who suggested that gamma functions provide the best fit to their extensive in situ database of cirrus particle size distributions. Gamma functions formally require estimation of three unknown parameters: a characteristic length scale, a characteristic concentration and an exponent that characterizes the standard deviation or breadth of the distribution. It has become customary to fix the exponent to some small integer value [*Matrosov et al.*, 1994; *Mace et al.*, 1998b]. The validity of this practice has not been thoroughly tested, however, although *Matrosov et al.* [1994] suggest that its overall influence on the uncertainty of the retrieval algorithm is small. Another factor not addressed in the present class of algorithms relates to the modality of particle size distributions in cirrus. Observations show that cirrus particle size distributions are often bimodal [*Mitchell*, 1996] with a large particle mode peaking in the 200–400 micron region and a smaller particle mode whose characteristics are largely unknown due to uncertainties in optical array probes. *Platt et al.* [1998] suggests that this bimodality be represented by a combined exponential function for the small particle mode and a gamma function for the large mode.

[9] Our goal in this work is to explore some of these issues and suggest an approach for retrieving the characteristics of cirrus using the radar reflectivity and Doppler velocity observed by vertically pointing millimeter-wavelength radar. This algorithm draws on recent advancements in approximately separating the air motions from the particle fall speeds in Doppler velocity data [*Orr and Kropfli*, 1999], of theoretically characterizing the fall speed and mass-dimensional relationships of several particle habits [*Heymsfield and Iaquinta*, 2000], and the manner in which cirrus clouds scatter microwave radiation [*Aydin and Walsh*, 1999]. To show the limitations imposed by our assumptions, we present an analysis of data from several research flights over the SGP ARM site in the section 2. A description of the algorithm and validation is presented in section 3. Further results and a discussion follow.

2. Analysis of Aircraft-Observed Particle Size Spectra

[10] Our goal is to develop an algorithm that can be applied to millimeter radar observations of ice-phase clouds in the upper troposphere (cirrus) where the clouds can exist above lower level clouds and/or have an IR emissivity approaching unity. Since only Doppler radar can effectively probe above lower level clouds and through optically thick ice clouds, we are practically limited to at most three observations in each radar resolution volume. These observations are the radar reflectivity, mean Doppler velocity and Doppler spectrum width (see section 3 for a discussion of our approach to expressing these quantities in terms of distributions of nonspherical ice crystals). Of these observations, only the radar reflectivity factor (Z_e) is independent of the air motions within the radar resolution volume. The Doppler velocity ($\overline{V}_d$) and spectrum width ($\bar{\sigma}_d$) are the result of a convolution of the turbulent spectrum and some mean vertical motion with the particle size distribution. Without the full Doppler spectrum from which $\overline{V}_d$ and $\bar{\sigma}_d$ are derived, it is impossible to rigorously deconvolve the air motions from the quiet air fallspeed of the cloud particles. Certain assumptions can, however, be applied to $\overline{V}_d$ for approximately separating the air and mean particle motions [*Orr and Kropfli*, 1999]. We shall discuss this technique in some detail below. The Doppler spectrum width, on the other hand, presents no similar straightforward technique for estimating a value that would be observed in nonturbulent air. In fact, recent work suggests that the Doppler Spectrum width may not be amenable to further analysis [*Danne et al.*, 1999], although we consider this subject below. We may be practically limited to two observations in each resolution volume and it is always true that the complexity of an algorithm increases substantially with the number of degrees of freedom available to it. It is important, therefore, to identify the most appropriate functional approximations for the cirrus particle size distribution and to carefully identify the limitations of these approximations with available observations.

[11] We use a record of cirrus in situ data that has been collected at the SGP CART site in recent years. This data is composed primarily of optical array probe data (Particle Measuring Systems (PMS) probes [*Heymsfield and Parrish*, 1986]). The cirrus cases analyzed here are listed in Table 1. The cases cover a wide range of conditions that are typical for middle latitude cirrus. In all cases, the clouds were sampled with a similar flight strategy; the aircraft started

Table 1. Cirrus Flight Days Used in the Validation Study

Date	Approximate Time	Approximate Vertical	Type
4/18/97	19:30–21:30	7–11 km	Jet streak
4/21/97	18:40–20:20	6–12 km	Unknown
9/16/97	16:00–19:00	7–14 km	Multilayer/Frontal
9/19/97	14:30–17:00	8–12 km	Multilayer/Frontal
9/26/97	17:30–21:59	6–12 km	Hurricane Remnants
5/2/98	00:00–03:00	5–13 km	Anvil
5/8/98	14:00–18:00	6–11 km	Orographic/Jet streak

either near cloud base or top and stepped up or down at approximately 300m increments after performing a level leg of approximately 20 km centered on the SGP ground site. The cloud layer was profiled in this way and then a spiral of approximately 5 km radius was conducted centered on the SGP site through the layer. The pattern was repeated as long as the cloud and aircraft fuel permitted. This sampling approach was used in order to generate an unbiased statistical sample of the layers so that comparison studies with ground-based instruments could be conducted. The 2DC processing software was built upon code developed at NCAR beginning in the mid-1970s [e.g., *Heymsfield and Parrish*, 1978]. The current software was developed for the Interactive Data Language (IDL) package. The particle dimension (L) is derived as the "true" maximum diameter, not the maximum diameter along the array or flight direction axes as previously done. Partially imaged particles, e.g., particles that obscured either or both end elements of the 2D array, were "reconstructed" [*Heymsfield and Parrish*, 1978] to yield their maximum dimension. The limitations of the PMS data are well known; the smallest crystals are undersampled ($\sim$50–150 μm) or not sampled at all (<50 μm). However, for most midlatitude cirrus, the mass distribution is weighted to crystal sizes of several hundred microns, and the majority of the optical opacity, while weighted towards smaller sizes than the mass, is reasonably well sampled by the PMS 2DC [*McFarquhar et al.*, 2000]. The PMS data we use in this study is certainly able to characterize the larger modes of the particle size distribution and thus can be used to examine the Doppler radar characteristics of the sampled cirrus volumes.

[12] Our objective here is to examine data collected in situ to determine what assumptions are most reasonable for developing a cloud property retrieval algorithm that meets our needs. Specifically, we would like to determine what functional approximations are required to reproduce the observed size distributions to within at least their observational uncertainty [*Larson et al.*, 1998]. To determine this, we employ a functional fitting approach where each 5-second averaged PMS 2DC size distribution is fitted with three functional approximations: a two-parameter zeroth order gamma (exponential) function $n_e(L) = N_e exp[-\lambda_e L]$, a modified gamma function [*Gossard*, 1994; *Mace et al.*, 1998b]

$$n_g(L) = N_g e^{\alpha_g} \left(\frac{L}{L_g}\right)^{\alpha_g} \exp\left[-\alpha_g \frac{L}{L_g}\right]$$

expressed in terms of the modal size of the distribution (i.e., N_g is the number of particles per unit volume per unit length at the size L_g where the function is a maximum), and a bimodal distribution composed of the summation of the exponential function for the smaller particle mode and the modified gamma function for the larger particle mode as suggested by *Platt* [1997]. In the above distribution functions, N_e is the intercept value of the exponential function (subscript e) and λ_e controls the slope of the distribution with particle size. For the modified gamma distribution (subscript g), N_g is the number of particles at the modal size $L_g$while α_g controls the breadth of the distribution. The fitting procedure is straightforward and attempts to minimize a fractional variance parameter (δ) between the fitted and observed particle spectra. δ is defined as

$$\delta = \sum_{n=0}^{3} \left(\frac{\left(\langle L_{obs}^n \rangle - \langle L_{fit}^n \rangle \right)^2}{\langle L_{obs}^n \rangle} \right)^{1/2}$$

where $\langle L^n \rangle = \int L^n n(L) dl$ is the nth moment of the particle spectrum.

[13] While all size distributions were fitted with exponential and modified gamma functions, only distributions that were evidently bimodal were treated as such. To test for bimodality, we examined the slope of the size dependent 2DC concentration. If a decrease in slope between two size bins was found that amounted to more than 25% of the slope between the next highest and lowest bins, the distribution was considered to be bimodal and a minimum in slope was found. The size bin associated with this minimum slope was specified as forming the joining point or shoulder between the two distribution modes. The larger mode was fitted first by searching for a local maximum at sizes larger than the shoulder bin. If no local maximum was found, the maximum was placed 1 bin larger than the shoulder size. The modified gamma distribution was then fitted to the large mode as described above by examining the variance in sizes larger than the shoulder size. The exponential part of the distribution was then found by subtracting the modified gamma concentrations from the observed concentrations; the exponential function was then fitted to these residuals using the procedure described above. Examples size distributions and associated fits are presented in Figure 1.

[14] These procedures were applied to all PMS data from the flights listed in Table 1. Since our goal is to establish what assumptions concerning the functional form of the particle size distribution are reasonable in developing a retrieval algorithm applied to Doppler radar data, we begin by considering under what circumstances the aircraft data suggest that more information is required than we have available in the three Doppler moments. Figure 2 shows the frequency of occurrence of bimodal size distributions in terms of temperature and calculated radar reflectivity. Using the definition of bimodality given above, we find that a large fraction of particle size distributions appear to have bimodal characteristics. This result is not surprising and has been the subject of recent research [*Mitchell et al.*, 1996]. We find that the frequency of bimodal size distributions increases from a small frequency of occurrence for observations with small radar reflectivity and low temperatures to nearly 100% frequency of occurrence for resolution volumes observed at temperatures warmer than -25°C and with radar reflectivity larger than -20 dBZ_e. We now define

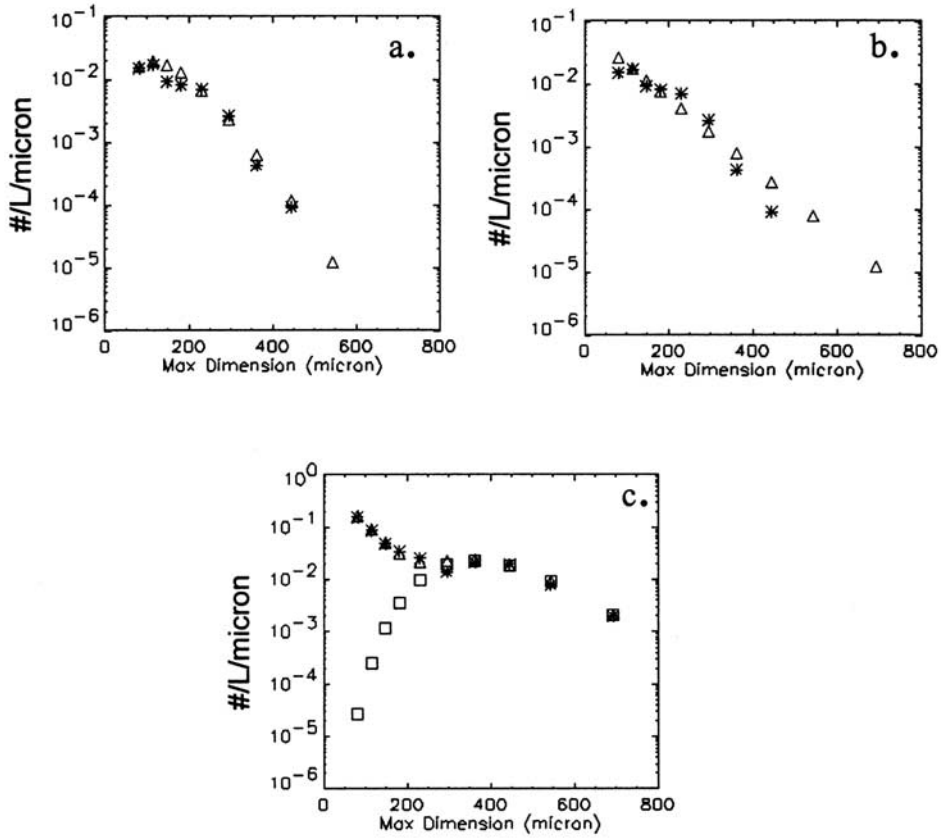

Figure 1. Particle spectra (denoted by the asterisks) collected above the SGP ARM site by the University of North Dakota Citation on 26 September 1997 in the remnants of Hurricane Nora [*Sassen et al.*, 2002]. The spectrum collected at 20:23:16 UTC shown in Figures 1a and 1b has an obvious difference in the rate of change of the particle number with size between the largest half and smallest half of the distribution. The modified gamma function (Figure 1a; triangles) with $\alpha = 3.5$ is best able to capture this characteristic. The exponential fit (Figure 1b; triangles) is unable to characterize both the large and small halves of this distribution and significantly overestimates the radar reflectivity and Doppler velocity and Doppler spectrum width. The distribution collected at 20:47:11 (shown in Figure 1c) is bimodal with the large particle mode peaking near 350 μm. In this case the modified gamma function with $\alpha = 10$ (shown as squares) combined with the exponential distribution (shown as triangles) is able to accurately model the observation.

those size distributions that have for the bimodal fit at least 50% smaller (i.e., better fit) than either the exponential fit variance parameter or the modified gamma fit variance parameter as being significantly bimodal. The value of 50% was chosen for two reasons. (1) Values such as IWC (second-third moment of the particle spectrum) are known to vary by a factor of 1000 in natural cirrus between 10^{-4} g m^{-3} and 10^{-1} g m^{-3} and (2) the uncertainty of parameters derived from measurements of particle spectra by PMS probes is on the order of 30–50% [*Larson et al.*, 1998]. We therefore define those distributions where $\delta_{bimodal} < 0.5\delta_{unimodal}$ as being significantly bimodal. If we then consider only those size distributions that are significantly bimodal, we find that many of the distributions that are bimodal by our initial definition are approximated to within observational uncertainty with unimodal functional forms (Figure 2b). This is especially the case when $Z_e < -5$ dBZ_e and $T < -25$ C. *Mace et al* [2001] using 1 year of MMCR data from SGP show that the majority (>80%) of isolated cirrus layers in the upper troposphere that would normally be defined as cirrus have $Z_e < -10$ dBZ_e and $T < -30$ C. Thus we conclude that a single-mode functional form requiring two or three independent parameters will be applicable to most cirrus observed at SGP with the MMCR within the T and Z_e ranges identified.

[15] The modified gamma function considered here has three degrees of freedom that results in significant flexibility; the functional maximum can be placed arbitrarily within the size domain and the breadth of the distribution can be adjusted to accommodate most physically realizable unimodal distributions. We found using the fitting procedure described above that for most single-mode particle size distributions, a modified gamma function could be fit to a level of accuracy often limited only by our desire to fine-tune the parameters. This flexibility, however, comes at a price. Using a fully defined gamma function in a retrieval

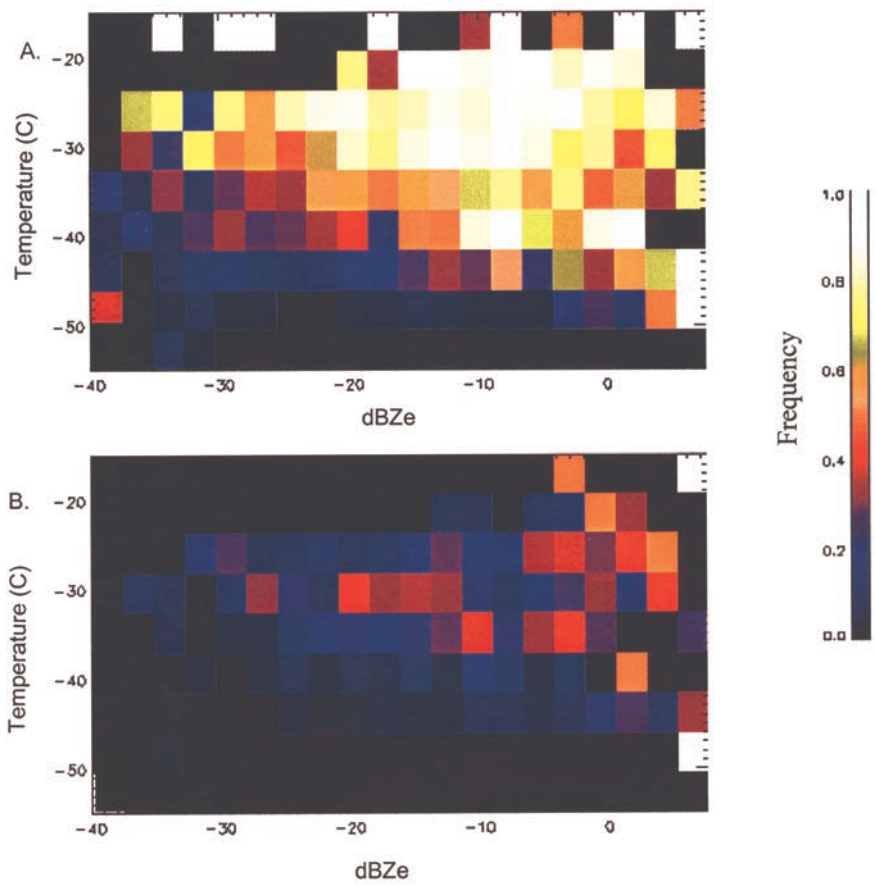

Figure 2. The frequency of occurrence of particle spectra that can be classified as bimodal (see text for definition) in terms of the temperature and the radar reflectivity at which the particle spectrum was collected. In Figure 2a are all data that show bimodal tendencies. In Figure 2b is the frequency of occurrence of particle spectra that are significantly bimodal. The text provides further details.

algorithm requires three independent sources of information about the crystal population within the resolution volume. It is important to determine if this degree of complexity is required or if simpler two-parameter functions provide a characterization of the cloud properties that is adequate with respect to our ability to observe them. The uncertainty in observing particle size distributions in cirrus clouds has recently been considered by *Larson et al.* [1998]. An optimistic interpretation of their results suggests that the mass and mean size derived from a well-calibrated PMS probe is generally on the order of 50% and 25%, respectively. In Figure 3, we plot the fractional error in mass and mean size incurred by fitting the approximately five thousand 5-second averaged particle spectra observed by the UND Citation with an exponential function using the fitting procedure described above. The error is plotted in terms of the mean and standard deviation of the error compiled in dBZ_e bins. We find that, in terms of mass, the mean error remains near 30% through Z_e values less than approximately -5 dBZ_e. When Z_e increases beyond -5 dBZ_e the exponential function is increasingly unable to characterize the mass to within reasonable accuracy. The precision of the functional fit also decreases as Z_e becomes larger as shown by the increasing standard deviation. This decrease in accuracy and precision is primarily due to bimodality of the particle spectra and due to the fact that the functional maximum of the spectra often moves to sizes greater than the smallest few bins of the 2DC probe. The mean particle size shows similar characteristics with decreasing accuracy and precision at larger Z_e values but acceptable performance below -5 dBZ_e.

[16] Figure 4 suggests that the exponential function is able through a decreasing slope to approximate the general broadening of the size distributions with temperature that is clearly evident in the fitted modified gamma functions. We find that in general the very narrow size distributions found at cold temperatures broaden substantially as the temperatures warm. Some caution should be exercised with the very narrow particle spectra at the cold temperatures since it is likely somewhat biased by the inability of the PMS 2DC to accurately characterize the smallest particles in the distribution. This factor would likely not change the qualitative tendency shown in Figure 4, however. The trend toward broader particle spectra can also be interpreted as a generally increasing mean particle size with temperature, a factor that is well documented in the literature [e.g., *Heymsfield and Platt*, 1984]. An evident scale break seems to be evident in the data collected near -35°C where $\alpha \sim 6$ changes rather abruptly to $\alpha \sim 1.5$. Interestingly, this is the approximate region that the *Heymsfield and Platt* [1984]

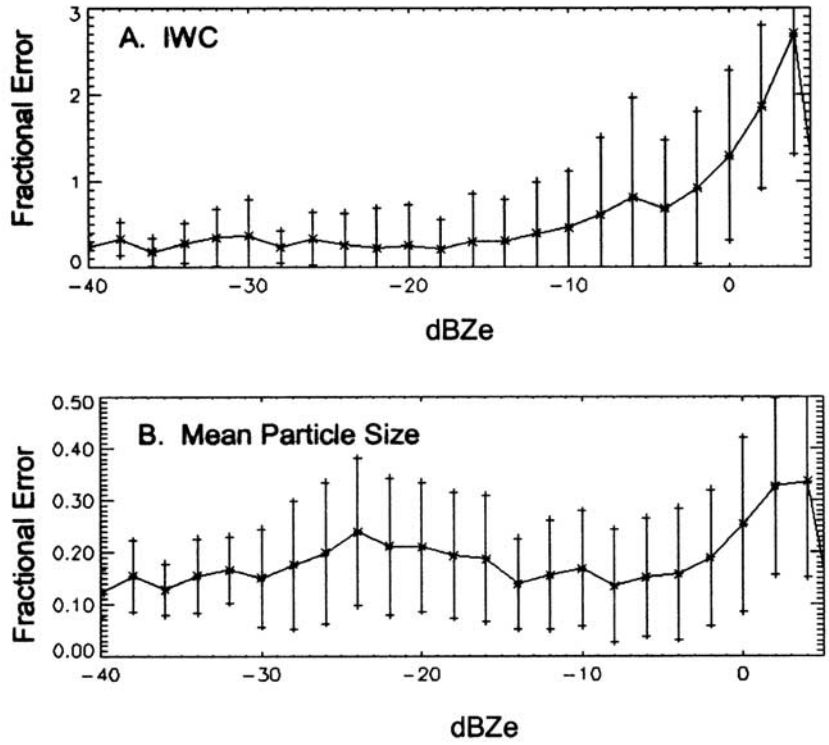

Figure 3. The mean absolute fractional error between properties of observed particle spectra and properties derived from a fit with an exponential function. Plotted are the mean values of the error in 2 dBZ_e bins. The error bars show 1 standard deviation from the mean of the error in each bin. (a) IWC, and (b) mean particle size.

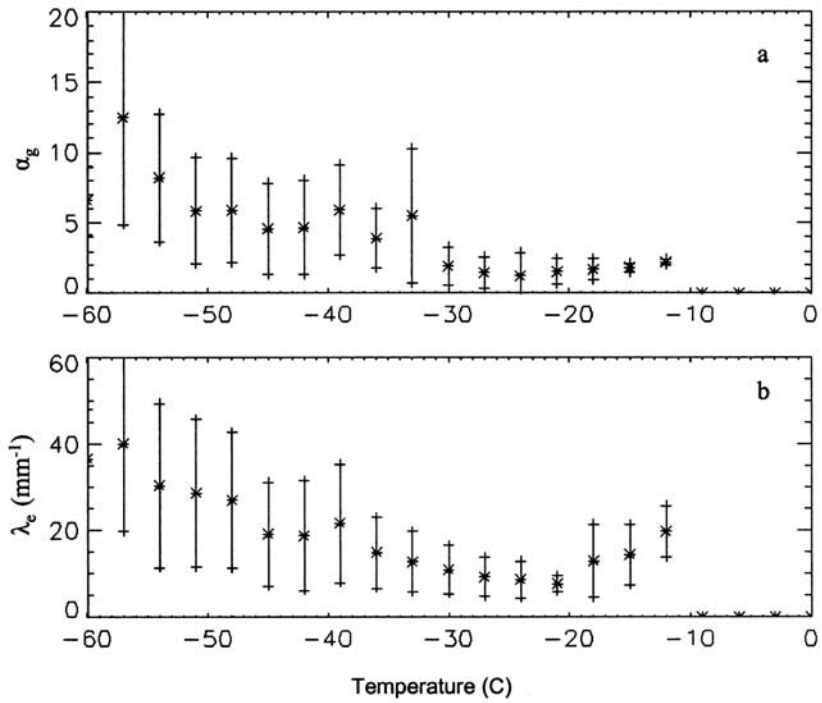

Figure 4. Behavior of (a) α_g from the modified gamma function fit to the observed particle spectra and (b) λ_e from the exponential function. Plotted are means (asterisks) and standard deviations (error bars) binned as a function of temperature in 3K increments.

data show a scale break in the *IWC* versus *T* relationship [see *Mace et al.*, 2001, Figure 1]. The slope parameter of the exponential function (λ_e) approximates this behavior of generally broadening size distributions but does not show the evident scale break found in the modified gamma fits. The increasing slope of the exponential size distributions at temperatures warmer that −20c is due to the fitting algorithm converging on the small particle mode of bimodal distributions.

3. Retrieval Algorithm

[17] For liquid cloud droplets of diameter D that are small compared to the radar wavelength, the backscatter cross-section per unit volume or radar reflectivity (η) can be expressed, $\eta = (\pi^5/\lambda^4)|k_w|^2 Z$ where Z is the radar reflectivity factor, when expressed in terms of spherical particles of diameter D, $Z = \int_0^\infty n(D)D^6 dD$, λ is the radar wavelength and k_w depends on the complex index of refraction for liquid water spheres [*Doviak and Zrnic*, 1993]. It is customary to express η in terms of the water equivalent radar reflectivity factor (Z_e) calculated from the backscattered power measured at the radar receiver [see *Doviak and Zrnic*, 1993, equation 4.35]. We choose to retain the definition of Z_e and to express the particle size distribution in terms of the maximum dimension, L, of nonspherical ice crystals since this is the quantity most readily measured by aircraft probes. We therefore write,

$$\int_0^\infty \sigma_b(L)n(L)dL = \frac{\pi^5}{\lambda^4}|k_w|^2 Z_e \tag{1}$$

where $\sigma_b(L)$ is the backscatter cross section of an ice crystal with maximum dimension, L. To relate the observations of radar reflectivity to the particle size distribution, we express equation (1),

$$Z_e = \gamma \int_0^\infty n(L)L^{6+\kappa}dL \tag{2}$$

where we have used

$$\gamma L^k = \frac{\sigma_b(L)\lambda^4}{L^6\pi^5|k_w|^2}.$$

The parameters γ and κ are found through a power law fit using a parameterization to σ_b described by *Aydin and Walsh* [1999] for bullet rosettes and hexagonal columns. The Doppler velocity, $\overline{V}_D$, and Doppler spectrum width, $\bar{\sigma}_d$, can then be expressed similarly,

$$\bar{V}_D = \frac{\gamma}{Z_e}\int_0^\infty V(L)L^{6+\kappa}n(L)dL, \tag{3}$$

$$\bar{\sigma}_D^2 = \frac{\gamma}{Z_e}\int_0^\infty (V(L) - \bar{V}_D)^2 L^{6+\kappa}n(L)dL. \tag{4}$$

In equations (3) and (4), $V(L)$ is the particle fallspeed that is defined using empirical data as described in the text.

[18] Using the moments of the Doppler spectrum to retrieve the microphysical properties of cirrus clouds has advantages but also poses challenges. One of the primary advantages of millimeter-wavelength radar is their capacity to quantitatively probe higher clouds through nonprecipitating cloud layers thereby making available for study a wide range of situations that have received relatively little attention up to now. In some regions like the Arctic, cirrus often occur above lower level overcast layers and exert a substantial perturbation on the column energy budget. Cloud layers in the upper troposphere can also be optically thick; particularly outflows from deep convection and regions associated with deepening frontal clouds. These situations have received relatively little attention in the literature since they present limitations to both observations by lidar and to algorithms that rely on observations of downwelling thermal IR.

3.1. Accounting for Air Motions

[19] Before reduction into the moments of the Doppler spectrum, Doppler radar power spectra record information on the energy backscattered from hydrometeors as a function of radial velocity. If the radar is pointing vertically and the particles are falling through nonturbulent air that is motionless along the vertical direction, the number of particles in a velocity bin can be estimated from the received power. The condensate mass in the resolution volume could then also be calculated. In most circumstances, however, the air motions have sufficient magnitude to influence the vertical motions of the particles. The convolution of the turbulent spectrum with the particle fallspeed spectrum results in the loss of any straightforward quantitative interpretation of the Doppler power data. Techniques have been developed to treat Doppler spectra collected in liquid-phase clouds [*Gossard*, 1994; *Babb et al.*, 2000], however, these techniques have not yet been applied to cirrus. Furthermore, most radar systems do not routinely record Doppler spectra; the data are typically reduced automatically to their first three moments (see equations (1)–(4)) due to data volume considerations.

[20] Vertical air motions that are significant with respect to the fallspeed of cirrus cloud particles occur over a continuum of spatial and temporal scales. Those motions that fluctuate on scales much smaller than the resolution volume of the radar (a few tens of meters) broaden the observed Doppler power spectrum [*Gossard*, 1994; *Doviak and Zrnic*, 1993] while vertical air motions that occur on scales greater than the temporal and spatial resolution of the radar observation tend to cause the velocity spectrum to shift by an amount proportional to the air motion magnitude. We can further separate these larger-scale motions into those that occur on spatial and temporal scales that are small with respect to the cloud system (we define these as internal to the cloud system) and those whose scale tends to be comparable to or bigger than the cloud system (mesoscale to synoptic-scale motions; considered external to the cloud system). (By internal and external to the cloud system we mean, respectively, those scales of motion whose magnitude can and cannot be reduced substantially in magnitude by averaging over a reasonably long time period (∼1.5–2 hours). A similar definition is applied to vertical motions considered internal and external to individual observations

that have horizontal scales of ~10 m and temporal scales of ~10 s.) This conceptual classification of the vertical motion continuum is not unfamiliar to cloud system modelers who typically prescribe a large-scale ascent, allow the model dynamics to generate internal circulations, and parameterize turbulence using a closure assumption [*Starr and Cox*, 1985; *Gu and Liou*, 2000; *Lin*, 1997]. Since we cannot treat the full spectrum of vertical motion in a continuous sense as we could with full Doppler spectra, we adopt this conceptual scale separation as an approximation.

[21] The magnitudes of vertical air motions tend to be inversely proportional to the spatial and temporal scales of the motion. While few cases documenting the larger synoptic-scale vertical motions are available in the literature, the reported magnitudes are on the order of 2–3 cm s^{-1} either up or down at cirrus altitudes [*Starr and Wylie*, 1990; *Mace et al.*, 1995; *Heymsfield*, 1977]. Thus the larger mesoscale and synoptic-scale vertical motions are normally much smaller than the Doppler fall speed of most cirrus observed with cloud radar (greater than ~20 cm s^{-1}; *Matrosov and Heymsfield* [2000]). Cirrus cloud systems on the other hand show rather strong organization on the mesoscale [*Sassen et al.*, 1989], and we expect the vertical motions on these scales to be organized similarly. *Gultepe and Starr* [1995] analyzed vertical motions collected in situ and found that the aircraft observed leg-averaged (~20 km) vertical air motions ranged from −15 cm s^{-1} to +10 cm s^{-1} in one case (28 October 1988) and from −3 cm s^{-1} to −16 cm s^{-1} in another (19 October 1988) with bias errors on the order of 25 cm s^{-1}. The cirrus events we examine typically extend to temporal scales of several hours corresponding to length scales on the order of 100 km; several times larger than Gultepe and Starr's data length. Thus, based on Gultepe and Starr's values, it is reasonable to expect vertical motion magnitudes on the order of 10–15 cm s^{-1} as an upper limit for the vertical motion that we consider external to the cloud system. The important point to this reasoning is that the mesoscale vertical motions tend to be smaller than the minimum Doppler motions we observe in most cirrus layers, although, the bias error induced by these motions will be significant in some cases [*Heymsfield*, 1977].

[22] The motions that can be considered internal to the cloud system but external to the observations are the up- and downdrafts that form and maintain individual elements of the cloud system over its lifecycle. The magnitudes of these motions based on results presented by *Heymsfield* [1977] and *Gultepe and Starr*'s [1995] data where $w_t < \sim 50$ cm s^{-1} are substantial compared to cirrus particle fall speeds and cannot be neglected. Due to mass continuity however, we can assume that over some suitable averaging time these vertical motions will average to zero. *Orr and Kropfli* [1999] (hereinafter referred to as OK99) describe a technique to approximately remove these internal air motions from long records of Doppler radar data collected in cirrus by averaging. We adopt their conceptual approach here. The underlying assumption of this technique is that volumes with similar characteristics (which we will define) have similar particle size distributions and, therefore, have similar quiet air fall speeds. With this fundamental assumption it follows that if the Doppler velocities of these similar volumes are averaged over a sufficient time period, all but the motions external to the cloud system will be significantly reduced in magnitude compared to the quiet air Doppler velocity ($\overline{V}_d^q$) of the ice crystals. In practice, OK99 perform their averaging using a multiple linear regression algorithm with the radar reflectivity factor as the predictive variable and reason that the absolute accuracy of the quiet air fallspeeds are on the order of 10 cm s^{-1}. However, they presented no direct comparison to independent data for the cases they examined.

[23] The underlying assumption of the OK99 method needs to be carefully considered. We are essentially attempting to identify volumes that have similar particle size distributions of ice crystals and, therefore, reasonably similar $\overline{V}_d^q$. However, we have very little data that objectively discriminate between the relative microphysical properties of various cirrus volumes. The radar reflectivity factor, Z_e, (as surmised by OK99) is one such variable but, it is likely not entirely sufficient since Z_e is so heavily weighted by the largest particles in the size distribution (equation (2)). Consider, for instance, the possibility that a population of particles in the sublimation zone of a cirrus layer has the same radar reflectivity as particles in the depositional growth region of the layer. We would expect these two populations to have different terminal velocities even though they have the same radar reflectivity. To identify other possible predictive quantities to compliment Z_e, we adopt a classic view of cirrus layer structure [*Heymsfield*, 1975] where cloud particles are nucleated near cloud top in water saturated updrafts and grow in the updraft until they are detrained or gain sufficient mass to sediment. The particles continue to grow through vapor deposition and aggregation as they sediment through ice saturated layers below the nucleation zone until they reach a layer that is subsaturated with respect to ice where they begin to sublimate [*Heymsfield and Donner*, 1990]. It is reasonable to assume that, on average, the particle size distributions found within the layer will be correlated with the distance the particles have sedimented from near the nucleation zone and on the temperatures at which they have grown. Certainly, temperature and distance from layer top are themselves correlated with one another. However, these information sources do contain some amount of independent data about the cloud properties as demonstrated in a layer-mean sense by *Mace et al.* [2001] where it was shown that both layer thickness and layer-mean temperature are useful in understanding the microphysical properties of cirrus layers. Therefore we include the temperature (T) and the vertical distance of the cirrus volume from the layer top (Δ) along with Z_e as the set of properties that together define volumes with similar particle size distributions and, by assumption, similar quiet air Doppler velocities. Given a sufficient number of observations within this three dimensional parameter space, we assume that the variability in the data about some mean Doppler velocity obtained through multiple linear regression is due to random turbulent air motions and that the mean value is the quiet-air Doppler velocity ($\overline{V}_d^q$) we seek.

[24] We also consider the spectral width (square root of the second moment of the Doppler spectrum). Making the same fundamental assumption; volumes with similar characteristics (Z_e, T, Δ and we now add $\overline{V}_d^q$) are expected to have similar quiet air Doppler spectral widths ($\bar{\sigma}_d^q$). However, since air motions that occur on scales smaller than the

Table 2a. Statistics of the Regression Coefficients Found From the Linear Regression Algorithm Described in the Text[a]

	C_0		C_Z		C_T		C_Δ		C_V	
	Mean	SDV	Mean	SDV	Mean	SDV	Mean	SDV	Mean	SDV
$\overline{V}_d^q$	0.82	0.52	1.8e-2	8.1e-4	−1.7e-3	1.1e-2	2.1e-2	6.6e-2	N/A	N/A
$\bar{\sigma}_d$	−1.1e-6	9.1e-6	−3.3e-3	2.9e-3	−1.3e-4	2.4e-3	−3.1e-3	2.4e-3	0.21	0.19

[a]The symbols listed here are explained in the discussion of equation (5).

temporal and spatial scales of the observations only act to broaden the Doppler spectrum [*Gossard*, 1994], we cannot invoke mass continuity, and, therefore, averaging would not lead us to the quiet air values we seek. Therefore we assume that those resolution volumes with similar cloud characteristics that have the smallest observed spectral widths are those least affected by turbulence. We organize the resolution volumes covering the cloud event into discrete reflectivity and temperature bins 2 dBZ_e and 2 K wide, and identify the 5% of observations in each well-populated bin that have the smallest spectral widths. This subset of data are then used with the multiple linear regression algorithm to derive a set of regression coefficients from which we estimate $\bar{\sigma}_d^q$ for every resolution volume in the cloud event based on the observed $Z_{e,}$, T, Δ and derived $\overline{V}_d^q$.

[25] To summarize, following *Orr and Kropfli* [1999], multiple linear regression is used to estimate $\overline{V}_d^q$ and $\bar{\sigma}_d^q$ with equations of the form,

$$\begin{aligned} \bar{V}_d^q &= C_{0V} + C_{ZV} dBZ_e + C_{TV} T + C_{\Delta V} \Delta \\ \bar{\sigma}_d^q &= C_{0\sigma} + C_{Z\sigma} dBZ_e + C_{T\sigma} T + C_{\Delta\sigma} \Delta + C_{V\sigma} \bar{V}_d^q \end{aligned} \quad (5)$$

where C denote regression coefficients and subscripts, $0,Z,T,\Delta$, and V denote coefficients multiplying the observations of dBZ_e, T, Δ, and $\overline{V}_d^q$, respectively. In equation (5), $\overline{V}_d$ is expressed in units of m s^{-1} and $\bar{\sigma}_d^q$ in m s^{-1}. The inputs are as follows; dBZ_e has units of 10 * $\log_{10}(Z_e)$ where Z_e is mm^6 m^{-3}, T is in Kelvins, and Δ is expressed in km. Table 2a provides a summary of the regression coefficients derived from approximately 150 cirrus events collected over 2.5 years at the SGP ARM site. It is interesting to note that the equation for $\overline{V}_d^q$ is largely determined by C_{0V} and C_{ZV} since for typical values of temperature and cloud layer depth, the last two terms on the right are small and tend to cancel. Also, observe from Table 2a that C_{ZV} is effectively constant from case to case while C_{0V} varies substantially. Table 2b lists the correlation coefficients of the predictor variables with $\overline{V}_d$ and $\bar{\sigma}_d^q$. We find that for $\overline{V}_d$, the correlation with Z_e is positive and large compared to the weaker correlations found with T and Δ. Strong negative correlations are found between $\bar{\sigma}_d$ and Z_e and T. The negative correlation between $\bar{\sigma}_d$ and Z_e is particularly interesting since it implies that as Z_e increases, the Doppler spectra is more dominated by a large particle mode and therefore is more peaked. We will return to this table later when we discuss validation and implementation of the retrieval algorithm.

[26] OK99 examine the sensitivity of this technique applied to $\overline{V}_d$ to variables such as uncertainty in the velocity data and averaging time and reason that the absolute accuracy of $\overline{V}_d^q$ is better than 10 cm s^{-1}. We attempt to establish the uncertainty of this algorithm using aircraft data. Figure 5 shows data from a cirrus event that was sampled by remote sensors and aircraft on 9 March 2000 [*Heymsfield et al.*, 2002] during the spring 2000 cloud Intensive Observing Period (IOP) at the SGP ARM site. Figure 5a shows the Z_e time-height cross section along with the aircraft track. While Figures 5b and 5d show, respectively, the $\overline{V}_d$ and $\overline{V}_d^q$ while Figures 5c and 5e show $\bar{\sigma}_d$ and $\bar{\sigma}_d^q$. This cirrus cloud field formed in association with a propagating disturbance embedded in the mid latitude jet stream and propagated over the surface instruments as a series of bands oriented along the wind where each band became progressively thicker. The first of these bands occurred at 19:26 UTC, the second at 20:24 UTC and the third near 21:36 UTC. Inspection of the unfiltered Doppler velocity data (Figure 5b) show that much of the layer, even those portions with very low reflectivity, was descending at more than 50 cm s^{-1}. We also find that the regions near the center of the high reflectivity fall streaks tended to have higher Doppler velocity (>1 m s^{-1}). In implementing the regression algorithm we weight the relative uncertainty in the Doppler velocity based on the magnitude of Z_e and based on $\bar{\sigma}_d$ (narrower spectra are expected to be least influenced by turbulence and, therefore, would tend to have more precise $\overline{V}_d$). For resolution volumes whose $\bar{\sigma}_d$ values were less than 0.25 m s^{-1}, the assumed uncertainty in the Doppler velocity are varied linearly from an estimated 10% for reflectivity values greater than −20 dBZ_e to 100% for values less than −40 dBZ_e. Resolution volumes where $\bar{\sigma}_d$ was greater than 0.25 m s^{-1} were considered highly uncertain due to turbulent broadening of the Doppler spectra and assigned an error of 100%. This relative error weighting forces the regression algorithm to weight more heavily the observations that had strong signal in relatively nonturbulent air. We can see that a substantial portion of the cloud had Z_e greater than −20 dBZ_e so that the amount of information is not severely limited in this case. The result is to shift the event-averaged Doppler velocity from 67 cm s^{-1} (positive velocities are downward) before averaging to 42 cm s^{-1} after averaging.

[27] The observed second moment data in Figure 5c suggest a somewhat bimodal distribution of $\bar{\sigma}_d$ with most of the turbulent regions characterized by $\bar{\sigma}_d > 0.35$ m^2 s^{-2}

Table 2b. Means and Standard Deviations of the Correlation Coefficients Between $\overline{V}_d$ and the Predictor Variables and $\bar{\sigma}_d$ and the Predictor Variables[a]

	Z_e		Temperature		Δ		$\overline{V}_d^q$	
	Mean	SDV	Mean	SDV	Mean	SDV	Mean	SDV
$\overline{V}_d$	0.59	0.17	0.25	0.17	0.29	0.18	N/A	N/A
$\bar{\sigma}_d$	−0.77	0.33	−0.86	0.26	0.72	0.26	0.78	0.44

[a]The symbols listed here are explained in the discussion of equation (5).

and the non turbulent regions characterized $\bar{\sigma}_d < 0.20$ m^2 s^{-2}. We also find that the apparently turbulent regions seem to be concentrated near cloud base and cloud top presumably where turbulent entrainment of noncloudy air is occurring across inversions. These regions may also be related to a partial filling of the radar beam near the cloud edges.

[28] During this cloud event the University of North Dakota Citation flew 75 km along wind legs from southwest to northeast centered on the ARM site. Particle spectra observations were compiled from the 2DC and 2DP PMS probes during these legs and merged into particle size distributions according to the technique described by *Heymsfield and Parish* [1978]. We use the observed size distributions as a means of testing the algorithm described above for separating the air and particle components of the first and second Doppler moments. Figure 6 shows schematically the procedure we use for evaluating the technique. Moving along the processing path labeled as 1A–3A in Figure 6, the Ka band Doppler moments were calculated from the in situ probe data using equations (2)–(4) with the *Heymsfield and Iaquinta* [2000] terminal velocity relationship and the *Aydin and Walsh* [1999] backscatter cross section parameterization for bullet rosettes. We will refer to these derived values as $Z_{e,A}$, $\bar{\sigma}^q_{d,A}$, and $\overline{V}^q_{d,A}$ where the additional subscript A has been added to signify quantities calculated from aircraft-observed particle spectra. Now along the path labeled 1B–3B (path B), the regression coefficients for equation (1) were determined normally from the MMCR-observed Doppler moments data using the technique described above. Then, $\bar{\sigma}^q_d$ and $\overline{V}^q_d$ were calculated by moving along path C where $Z_{e,A}$, T_A, and Δ were used as input to the regression equations with coefficients derived from along path B. $\bar{\sigma}^q_d$ and $\overline{V}^q_d$ were then compared to $\bar{\sigma}^q_{d,A}$ and $\overline{V}^q_{d,A}$. The renditions of $\overline{V}^q_d$ and $\bar{\sigma}^q_d$ compared in Figure 7 are essentially independent estimates of the same quantities except for the use of Z_{eA} in step 1C and the sixth moment weighting applied in step 2A. Since the regression coefficient derived in step 3B and applied in step 1C are totally independent of the aircraft data, the comparison shown in Figure 7 provides a valid test of the technique. We find that both $\overline{V}^q_d$ and $\bar{\sigma}^q_d$ are correlated with $\overline{V}^q_{d,A}$ and $\bar{\sigma}^q_{d,A}$ with minimal bias. The scatter evident in Figure 7 is not due only to the error in the regression-derived values but also due to the uncertainty in calculating $\overline{V}^q_{d,A}$ and $\bar{\sigma}^q_{d,A}$ from coarsely resolved aircraft size spectra. Thus the RMS of 20% and 40% for $\overline{V}^q_d$ and $\bar{\sigma}^q_d$, respectively, can be considered upper bounds for this case. Clearly, more comparisons like this are necessary. We address additional issues related to this technique when we discuss overall implementation of the retrieval algorithm below.

3.2. Forward Calculations

[29] It appears reasonable to assume (with limitations) that cirrus particle spectra can be characterized to within realistic observational uncertainty by single-mode exponential functions, and that the coefficients required to determine these functions for a particular sample volume can be acquired from observations of Z_e and, with sufficiently careful data analysis, of $\overline{V}_d$. Assuming an exponential size distribution of particles and power law representations for the fall speed, these equations can be written,

$$\begin{aligned} Z_e &= N_e\gamma \int_0^\infty L^{6+\kappa}\exp(-\lambda_e L)dL \\ \bar{V}^q_d &= \tfrac{a\gamma N_e}{Z_e}\int_0^\infty L^{6+\kappa+b}\exp(-\lambda_e L)dL \\ \bar{\sigma}^q_d &= \tfrac{\gamma N_e}{Z_e}\int_0^\infty \left(aL^b - \bar{V}^q_d\right)^2\exp(-\lambda_e L)dL \end{aligned} \tag{6}$$

where a and b are coefficients dependent on particle habit that describe a power law relationship between the particle terminal velocity and the particle maximum dimension; $V_{particle} = aL^b$. Other symbols were defined earlier. Additionally, we define the following basic microphysical parameters,

$$\begin{aligned} IWC &= mN_e\int_0^\infty L^n\exp(-\lambda_e L)dL \\ N_T &= N_e\int_0^\infty \exp(-\lambda_e L)dL \\ 0.5 &= \frac{mN_e\int_0^{L_{MM}} L^n\exp(-\lambda_e L)dL}{IWC} \end{aligned} \tag{7}$$

where IWC is the ice water content (g m^{-3}), N_T is the particle concentration (l^{-1}), L_{MM} is the mass median particle length (μm). In equation (7), n and m are coefficients of a power law relationship that relate the maximum particle dimension to the mass of the particle. Obviously, the coefficients n and m, like those for the fallspeed and backscatter cross section, are empirically determined functions of particle habit (Table 3 lists the coefficients used in this paper for bullet rosettes). Formulating our forward model equations in terms of power law relations allows some flexibility for developing solutions for different particle habits, updated information regarding the dimensional relationships, or for cases that are well-documented with aircraft data.

[30] The retrieval process essentially entails determining an appropriate N_e and λ_e in terms of the measured Z_e and derived $\overline{V}^q_d$. We adopt a straightforward numerical solution approach where for a wide range of N_e and λ_e, we calculate Z_e and $\overline{V}^q_d$ (equation (6)) and the microphysical parameters associated with the distribution listed in equation (7). Then a lookup table is constructed by interpolating values of N_e and λ_e and the microphysical parameters defined in equation (7) to a grid of Z_e and $\overline{V}^q_d$ values. While more precise numerical approaches could be employed, we are justified in using this technique because the primary uncertainty in this algorithm comes through measurement errors, the habit assumptions and the associated empirical relationships as we demonstrate below.

[31] To gauge the validity of the numerical technique, we use the particle spectra data sets described above. The size distributions are converted to $Z_{e,A}$ and $\overline{V}^q_{d,A}$ using the empirical relations given above and the microphysical parameters described in equation (7) are calculated directly from the observed size distributions. A lookup table is then used to retrieve simulated exponential distributions and associated microphysical parameters from $Z_{e,A}$ and $\overline{V}^q_{d,A}$. The values extracted from the lookup table are compared to

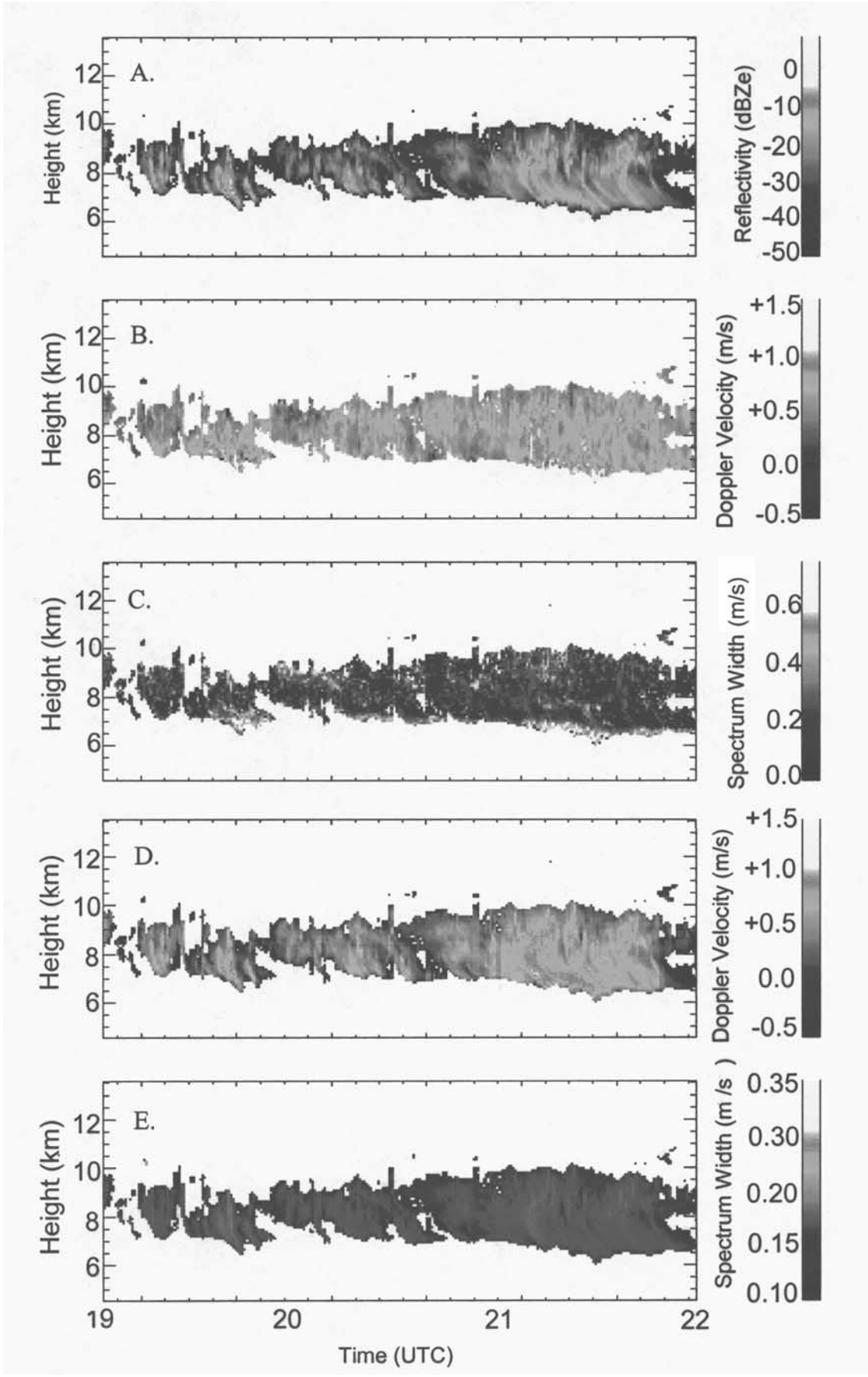
A.
B.
C.
D.
E.
Height (km)
12
10
8
6
Reflectivity (dBZe)
0
-10
-20
-30
-40
-50
Doppler Velocity (m/s)
+1.5
+1.0
+0.5
0.0
-0.5
Spectrum Width (m/s)
0.6
0.4
0.2
0.0
Spectrum Width (m /s)
0.35
0.30
0.20
0.15
0.10
19
20
21
22
Time (UTC)

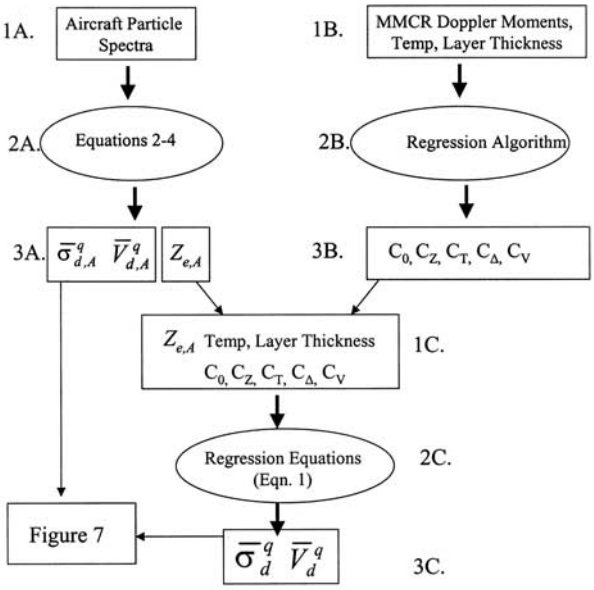

Figure 6. Schematic illustrating the procedure leading to the results shown in Figure 7.

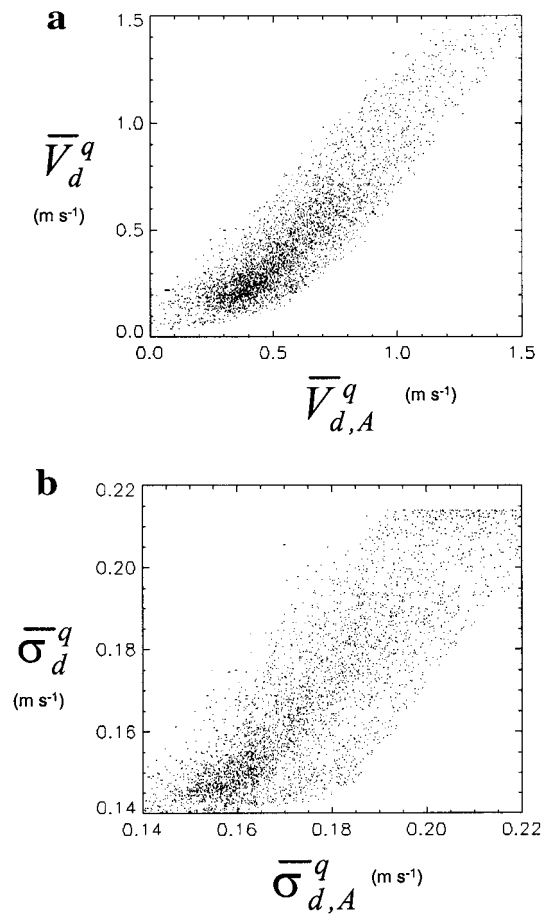

Figure 7. (a) Correlation plot of the quiet air Doppler velocity derived from observed particle spectra (abscissa) to the quiet air Doppler velocity calculated using the MMCR-derived regression coeffecients (ordinate). (b) As in Figure 7a, except for the quiet-air Doppler spectrum width.

those derived directly from the particle spectra. Figure 8 and Tables 4a and 4b show the results of the comparison. The microphysical data are well characterized by the algorithm with error arising principally from the coarse spectral resolution of the PMS data. Since no measurement or empirical uncertainties are included in this comparison, we consider the error values shown here to be due only to the numerical approach representing theoretical error minimums that will not be realized in practice.

3.3. Sensitivities

[32] In evaluating the utility of this algorithm, several sources of uncertainty must be considered. Based on the analysis presented in section 2, we can expect uncertainties on the order of 20% in $\overline{V}_d^q$ and error can be anticipated in Z_e due to absolute calibration of the radar and due to such factors as cloud inhomogeneity and partial beam filling across the radar resolution volume. Additionally, the lookup tables that we are constructing are currently valid for only a single or fixed weighted combination of particle habits. Natural cirrus can be composed of many different particle habits (as well as aggregates of these habits) the exact combination of which cannot necessarily be determined using routinely available ground-based data. This mix of particle habits and our inability to ascertain which habits might be occurring in a particular volume at a particular time leads to uncertainty in the retrieved quantities. These two sources of error will be examined separately and then the overall uncertainty due to their combination will be considered.

3.3.1. Sensitivity to Particle Habit

[33] The terminal velocity of a particle falling through a viscous medium is determined through a balance between the aerodynamic drag force and the acceleration due to gravity. It has been shown that this balance can be represented in terms of the ratio of the area that the particle projects to the airstream and the particle mass [*Mitchell*, 1996]. In water clouds where droplets are reasonably approximated as spheres or oblate spheroids, this ratio is easily represented in terms of a droplet dimension. In cirrus clouds where particles can assume several particle habits as well as aggregates of these habits, the relationship between the mass and projected area becomes more complicated. The choice of which area to mass ratio relationship is most appropriate in a given circumstance can be estimated but the choice is usually not clear. Furthermore, the relationship

Figure 5. (opposite) Height-time sections of the Doppler radar data observed by the MMCR on 9 March 2000 at the SGP ARM site. (a) Radar reflectivity, (b) unfiltered Doppler velocity (positive down), (c) unfiltered Doppler spectrum width, (d) Doppler velocity after application of our implementation of the Orr and Kropfli (1999) algorithm as described in the text, and (e) Doppler spectrum width after application of filtering algorithm. Note the different color scales used in Figures 5c and 5e.

Table 3. Coefficients of the Power Law Relationships Used When Assuming Bullet Rosette Particle Habits

	Coefficient	Value
Backscatter cross section (mm^2) Power law[a] (L in mm)	Γ	4.9e-5
	K	5.09
Fall Speed Power Law[b] (cgs units)	A	2150 ($L < 600$ μm), 492 ($L > 600$ μm)
	B	1.23 ($L < 600$ μm), 0.70 ($L > 600$ μm)
Mass Power Law[c] (cgs units)	m	1.2e-5 ($L < 90$ μm), 4.0e-4 ($L > 90$ μm)
	N	1.52 ($L < 90$ μm), 2.27 ($L > 90$ μm)

[a]Taken from *Aydin and Walsh* [1999, Table 1] for the 6–90 low density bullet rosette.
[b]Taken from *Heymsfield and Iaquinta* [2000, Appendix A, part 5f].
[c]Taken from *Heymsfield and Iaquinta* [2000, Appendix A, part 3a].

between the mass of the particle and its maximum dimension is also a strong function of particle habit. These issues obviously have direct and significant bearing on the algorithm we are evaluating. Fortunately, several studies reporting updated empirical relationships have appeared in the literature in recent years [*Heymsfield et al.*, 2002; *Heymsfield and Iaquinta*, 2000; *Mitchell*, 1996]. These studies can be used in the development of retrieval lookup tables for various pristine and weighted combinations of particle habits. The approach for picking the appropriate habit-dependent lookup table is still being developed although techniques that depend on temperature, radar reflectivity and synoptic situation seem to hold promise based on reported in situ data. In this paper our goals are less ambitious, and we currently just seek to examine the algorithm response and sensitivity to several pristine particle habits commonly observed in cirrus.

[34] Figures 9 and 10 show the behavior of the algorithm for typical ranges of Z_e and $\overline{V}_d^q$ for bullet rosettes (Figure 9) and hexagonal columns (Figure 10). The mass and fallspeed relations are taken from *Heymsfield and Iaquinta* [2000] and the radar backscatter is modeled using the parameterizations reported by *Aydin and Walsh* [1999]. The differences in the microphysical properties are shown in Figure 11. For both particle habits, we find that the ice water content and number concentration (not shown) are more or less equally dependent on the input variables while the particle size is dependent on $\overline{V}_d^q$. For this range of Z_e and $\overline{V}_d^q$ the values of *IWC* range from less than 10^{-4} g m^{-3} to just greater than 10^{-2} g m^{-3}. The number concentrations range from just a few per liter to several hundred particles per liter, and L_{MM} ranges from approximately 100 μm to near 600 μm. At a given Z_e, the *IWC* shows a greater absolute sensitivity of about a factor of 10 to Z_e between −25 and −15 dBZ_e. This is consistent with the variability found in published *Z-IWC* regression relations [*Atlas et al.*, 1995; *Liu and Illingworth*, 2000]. The differences between bullet rosettes and hexagonal columns are not immediately obvious when comparing the two plots due to the broad dynamic ranges in the microphysical parameters. Both habits respond in a similar fashion to the input variables and have similar ranges for the variables plotted here. The quantitative differences, however, are significant. We find that for a given reflectivity, assuming bullet rosettes results in a larger value of IWC by an amount that depends on $\overline{V}_d^q$. For $\overline{V}_d^q < 0.6$ m s^{-1}, the difference in *IWC* is less than a factor of two but increases rapidly to a factor of 4 as $\overline{V}_d^q$ increases to near 1 m s^{-1}. The difference in *IWC* is partially compensated by the fact that assuming columns results in more particles at a generally smaller size. The concentration difference (not shown) is largest at the smallest $\overline{V}_d^q$ and can be as large as a factor of 3 for $\overline{V}_d^q < 0.4$ m s^{-1}. The differences in L_{MM} tend also to be largest at the smallest $\overline{V}_d^q$ with magnitudes of the differences in the 30% range.

[35] To understand better the sensitivity of the algorithm in natural cirrus where particle habits are often mixed and occur somewhat at random, we return to the PMS data

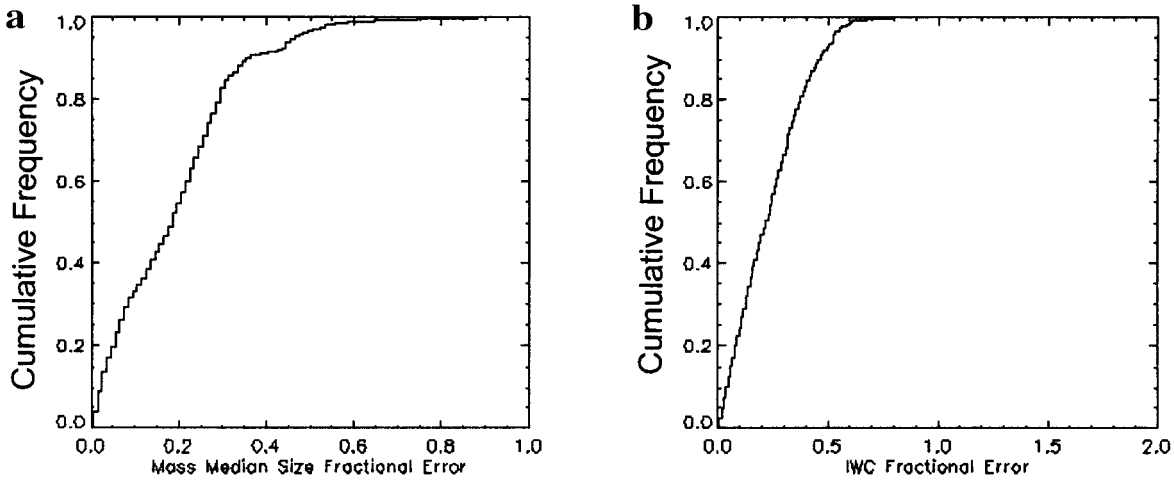

Figure 8. Cumulative error statistics assuming no observational error. Error shown here arises because of (1) numerical technique and (2) approximating continuous functions with coarse particle spectra. A point on either curve indicates that fraction of all cases (shown on the ordinate) with error less than the amount on the abscissa. (a) The cumulative error frequency for the mass median particle size, and (b) similar statistics for the ice water content. The fractional error is just the absolute value of the difference between the retrieval and the observation normalized by the observation.

Table 4a. Sensitivity of the Retrieved IWC to Uncertainty in Z_e and $\overline{V}_d^{q\mathrm{a}}$

	Radar Reflectivity Uncertainty, dB				
Sensitivity Parameter	0	2	4	6	8
Velocity Uncertainty 60%					
Median fractional error	0.46				
Correlation coefficient	0.74				
90th fractional error percentile	1.71				
95th fractional error percentile	2.55				
Velocity Uncertainty 50%					
Median fractional error	0.46				1.4
Correlation coefficient	0.74				0.40
90th fractional error percentile	1.71				>3.0
95th fractional error percentile	2.55				>3.0
Velocity Uncertainty 40%					
Median fractional error	0.39			1.23	
Correlation coefficient	0.79			0.49	
90th fractional error percentile	1.44			>3.0	
95th fractional error percentile	2.12			>3.0	
Velocity Uncertainty 30%					
Median fractional error	0.34		1.10		
Correlation coefficient	0.84		0.52		
90th fractional error percentile	1.24		>3.0		
95th fractional error percentile	1.81		>3.0		
Velocity Uncertainty 20%					
Median fractional error	0.28	0.62			
Correlation coefficient	0.89	0.51			
90th fractional error percentile	0.91	1.93			
95th fractional error percentile	1.28	2.85			
Velocity Uncertainty 10%					
Median fractional error	0.23				
Correlation coefficient	0.96				
90th fractional error percentile	0.59				
95th fractional error percentile	0.74				
Velocity Uncertainty 0%					
Median fractional error	0.21	0.36	0.56	0.67	0.72
Correlation coefficient	0.98	0.82	0.63	0.54	0.51
90th fractional error percentile	0.45	1.14	2.47	>3.0	>3.0
95th fractional error percentile	0.52	1.59	3.0	>3.0	>3.0

[a]Each table element (Z_e, $\overline{V}_d^q$ pair) shows four sensitivity parameters: the median fractional error, the correlation coefficient, and the 90th and 95th fractional error percentiles or the fractional error below which 90 or 95% of the distribution exists.

described earlier. Using the basic approach that led to the error analysis in Figure 8, we assume that all particles are bullet rosettes where the microphysical properties $\overline{V}_d^q$ and have been modeled as before. For each observed size spectrum, we calculate $Z_{e,A}$, $\overline{V}_{d,A}^q$, and the microphysical properties are calculated from the aircraft observed particle spectra using one of eight mass and area empirical relationships taken from *Mitchell* [1996] and listed in Table 5. The habit dependent empirical relationship used for any given size spectrum is determined from a uniform distribution of random numbers. The values of $Z_{e,A}$, $\overline{V}_{d,A}^q$ are then used as input to a lookup table constructed assuming bullet rosettes. Assuming bullet rosettes, $Z_{e,A}$, $\overline{V}_{d,A}^q$ are used to estimate the cloud properties. These properties are then compared to the "actual" properties calculated directly from the particle spectrum with random particle habits. The results of this exercise are shown in Figure 12. We find that randomly varying habits lead to a substantial increase in the uncertainty over that due only to the numerical approach. The median error in *IWC* increases to 54% while the uncertainty in particle size nearly doubles to 38%. The frequency of rather large errors in *IWC* and L_{MM} also increases with a 20% frequency of errors larger than 100%.

3.3.2. Sensitivity to Observational Error

[36] Like particle habit uncertainty, measurement error will increase the uncertainty in the microphysical retrievals over that presented in Figure 8. We know from the results presented earlier that converting $\overline{V}_d$ to $\overline{V}_d^q$ results in uncertainties of approximately 20%. The calibration of the MMCR radars at the ARM sites is generally known to within 1–2 dB [*Clothiaux et al.*, 1999; M. A. Miller, personal communication, 2001]. The microphysical properties derived from the particle size spectra are considered ground truth and $Z_{e,A}$, $\overline{V}_{d,A}^q$ are used to retrieve the microphysical parameters after an error increment is added to them. The error increment is determined using a normal distribution of random numbers centered on zero whose standard deviation is a predetermined magnitude. The microphysical parameters are extracted from the lookup tables using the perturbed values and compared to the ground truth data. The associated retrieval uncertainties

Table 4b. Sensitivity of L_{MM} to Uncertainty in Z_e and $\overline{V}_d^{q\mathrm{a}}$

Sensitivity Parameter	
Velocity Uncertainty 60%	
Median fractional error	0.26
Correlation coefficient	0.62
90th fractional error percentile	0.60
95th fractional error percentile	0.75
Velocity Uncertainty 50%	
Median fractional error	0.24
Correlation coefficient	0.64
90th fractional error percentile	0.54
95th fractional error percentile	0.67
Velocity Uncertainty 40%	
Median fractional error	0.23
Correlation coefficient	0.70
90th fractional error percentile	0.51
95th fractional error percentile	0.60
Velocity Uncertainty 30%	
Median fractional error	0.21
Correlation coefficient	0.73
90th fractional error percentile	0.47
95th fractional error percentile	0.56
Velocity Uncertainty 20%	
Median fractional error	0.19
Correlation coefficient	0.79
90th fractional error percentile	0.44
95th fractional error percentile	0.50
Velocity Uncertainty 10%	
Median fractional error	0.18
Correlation coefficient	0.84
90th fractional error percentile	0.41
95th fractional error percentile	0.47
Velocity Uncertainty 0%	
Median fractional error	0.18
Correlation coefficient	0.86
90th fractional error percentile	0.35
95th fractional error percentile	0.46

[a]Since L_{MM} is not a function of the reflectivity uncertainty, only sensitivity due to error in $\overline{V}_d^q$ is shown.

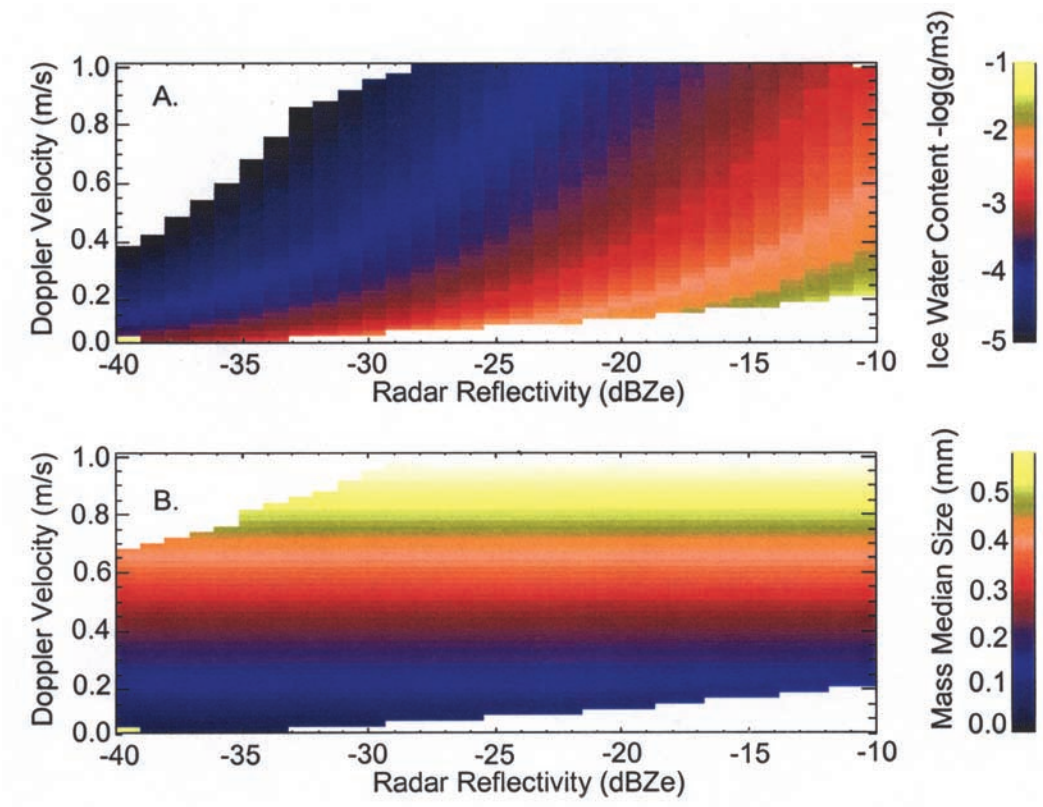

Figure 9. Algorithm response for input values of Doppler velocity and radar reflectivity assuming bullet rosette particle habits. (a) The IWC, and (b) the mass median particle size.

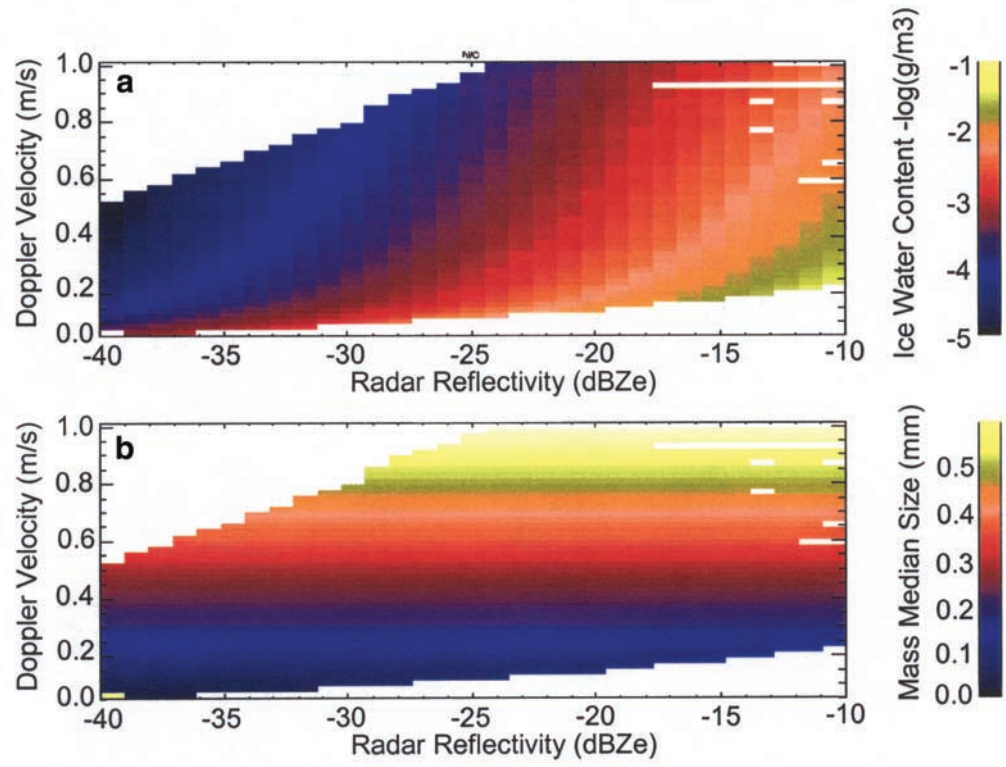

Figure 10. As in Figure 9, except assuming the particle habit is hexagonal columns.

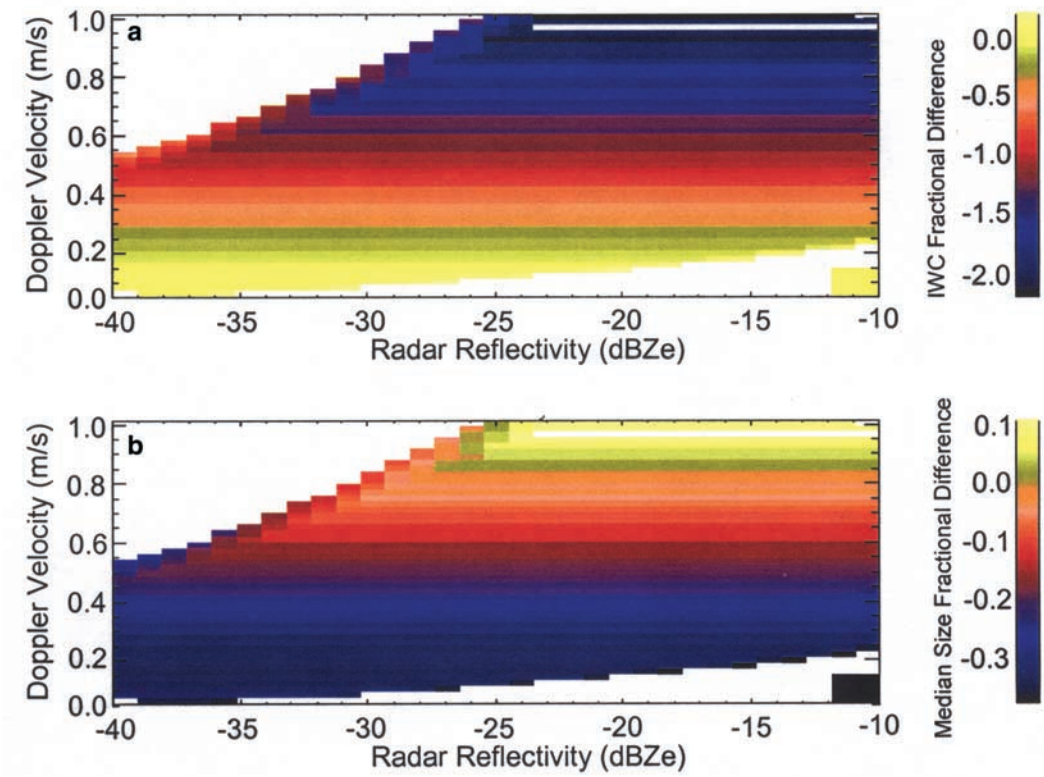

Figure 11. Differences between the values plotted in Figures 9 and 10. (a) The difference between bullet rosettes and columns as a fraction of the bullet rosette IWC. Negative values indicate the column IWC is larger. (b) As in Figure 11a, except for mass median particle size.

are listed in Tables 4a and 4b. We find that the algorithm is more sensitive to uncertainties in Z_e than to errors in $\overline{V}_d^q$. As we increase the radar calibration uncertainty from 1 dBZ_e to 6 dBZ_e we find the median error in retrieved *IWC* increases from approximately 20% to more than a factor of 2. For error in $\overline{V}_d^q$ increasing from 10% to 60%, the error in *IWC* increases only from 23% to 46%. Similarly, L_{mm} and N_t show a greater sensitivity to uncertainty in radar reflectivity. Combining uncertainties in Z_e and $\overline{V}_d^q$ is more realistic of actual data and results in a larger uncertainty in all retrieved quantities as listed in Table 4b and the diagonal elements of Table 4a. Finally, using the same general approach, we combine the error due to habit uncertainty with that due to observational error (20% for $\overline{V}_d^q$ and 2 dBZ_e for Z_e) to estimate the most likely retrieval error for this algorithm. When both of these error components are combined, we find that the median error in *IWC* increases to approximately 60% while the median error in L_{mm} and N_t increase to approximately 40% and 100%, respectively.

4. Comparison to In Situ Data

[37] The algorithm we are evaluating includes several assumptions that allow significant simplification to retrieving the properties of cirrus clouds. However, these simplifications come at a price as we have attempted to show with the sensitivity studies. The simplifying assumptions include assuming a single representative particle habit that exists in an exponential distribution of particles. We also assume that the air motion can be removed or separated from the Doppler velocity of the ice crystal population. We have shown that each of these assumptions as well as the numerical approach to solving the system of equations introduces some amount of error, but the error appears to remain within bounds that make the algorithm output sufficiently useful for cloud studies given the observed dynamic range of the cloud properties. Here we consider an additional test of the cloud property retrieval algorithm by comparing the derived properties directly to aircraft data. We use two basic approaches. The aircraft flights listed in Table 1 were conducted specifically for cloud property retrieval algorithm validation. Therefore we employ a point for point comparison of actual aircraft overpasses of the MMCR. The second

Table 5. Particle Habits Used in the Habit Sensitivity Experiment[a]

	Mass		Area	
Particle Type	m	n	ν	φ
Hexagonal Plates	0.00739	2.45	0.65	2.00
Hexagonal Columns	0.0010	1.9	0.051	1.41
Crystals with sector-like branches	0.0014	2.02	0.21	1.76
Side Planes	0.00419	2.3	0.229	1.88
Bullet rosettes	0.0031	2.26	0.087	1.6
Aggregates of side planes, columns and bullets	0.0028	2.1	0.229	1.88
Assemblages of planar polycrystals	0.0074	2.45	0.229	1.88

[a]The values of m, and n, ν, and φ, denote the parameters of power law relationships (mass = αL^{β} and Area = νL^{φ} where L is maximum particle dimension) in cgs units that relate the particle maximum dimension to the mass and projected area. This table has been adapted from Table 1 of *Mitchell* [1996].

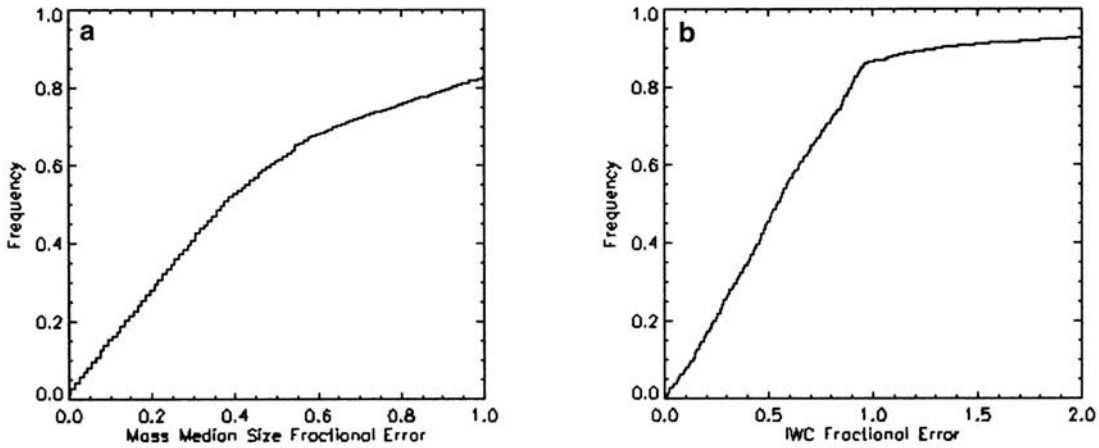

Figure 12. As in Figure 8, except the parameters retrieved assuming bullet rosettes are compared with values derived by randomly assuming one of the particle habits listed in Table 3.

approach will be more statistical and demonstrates a novel technique for cloud property algorithm validation using a combination of vertically pointing and scanning millimeter radar data.

4.1. Aircraft Overpass Comparison

[38] Comparing aircraft-observed microphysical data to ground-based radar data is always challenging due to the mismatch between the sample volumes of the two platforms and due to the natural heterogeneity in cirrus clouds. To provide an example, the MMCR at SGP has a field of view of approximately 0.19 degrees and a vertical resolution of 90m at cirrus levels. This equates to a sample volume at 10 km of 77×10^3 m^3. The PMS 2DC on the UND Citation has a sample volume rate of approximately 6 l s^{-1}. With a nominal airspeed of 100 m s^{-1}, the aircraft crosses the radar resolution volume in about 1/3 s during which it samples 2 l (0.002 m^3) of cloudy air. Obviously, with six orders of magnitude difference in sample volume between the in situ probe and radar, some form of averaging is needed when attempting to compare observations and retrievals for validation. As mentioned earlier, the majority of the aircraft missions were conducted using along-wind 20–30km straight horizontal flight legs that stepped vertically through the cloud layer. Finding a single optimal averaging length is likely not feasible due to differences in cloud properties from case to case and vertically from cloud base to top. One could easily imagine situations where a single 5-second averaged 2DC size distribution would be quite representative of the radar sample volume or on the other hand scenarios could be constructed where no amount of averaging of a horizontal aircraft leg would result in an appropriate characterization. Therefore, since our goal is to evaluate the skill of the retrieval algorithm with as much data as possible, we use a simple technique to estimate when the sample statistics of the radar reasonably matches that of the aircraft by comparing the observed and calculated radar reflectivity. First, cloud properties are determined using the retrieval algorithm with the MMCR-observed Z_e and derived $\overline{V}_d^q$. The value of Z_e for the radar sample volume nearest in time and space to an aircraft overpass is identified. Then, beginning with the value of $Z_{e,A}$ calculated from the in situ particle spectrum from the overpass point, $Z_{e,A}$ and Z_e are compared. If the values differ by more than 5 db, an additional 5-second averaged particle spectrum in the aircraft time series before and after the overpass point is included in the average spectrum to construct a size distribution from which $Z_{e,A}$ is re-calculated and then compared to Z_e. This procedure continues until a distance of 2 km from the radar is reached. If no averaged particle spectrum is found with a $Z_{e,A}$ within 5 db of Z_e, then we consider the aircraft and radar sample volumes to be mismatched and the overpass is discarded. Otherwise, the particular set of particle spectra that generate the closest agreement between the observed and calculated Z_e is considered the best possible match of sample volumes and the microphysical properties derived from this set of size distributions are used to compare with the retrieval algorithm results. While, using this technique will result in a natural correlation between the observed and calculated microphysical properties regardless of the degree of skill in the retrieval algorithm, we argue that this degree of correlation should only be as large as would be found in typical regression equations that relate, for instance, Z_e and *IWC*. According to *Atlas et al.* [1995], we would expect a standard error on the order of a factor of 2–3 for such comparisons.

[39] The comparison of *IWC* and L_{MM} for all matched volumes is shown in Figure 13, and certain error parameters are listed in Table 6. The observed *IWC* and L_{MM} values range over a factor of 100 and 4, respectively, indicating a wide range of cloud conditions sampled by the aircraft during the various flights. Since we are using the same mass-dimensional relations for the observed and retrieved data, these error statistics should be compared to Tables 4a and 4b. The *IWC* appears to be much better determined with this algorithm than is possible through regression relations with median errors in the 50% range. L_{MM} is also retrieved with reasonable skill; the median error is near 30% for this set of aircraft measurements. We note that there is some tendency for the retrieved values of L_{MM} to depart substantially from the observations in cases where the observed L_{MM} is large. This is due in part to the inability of the algorithm to characterize bimodal particle size distributions.

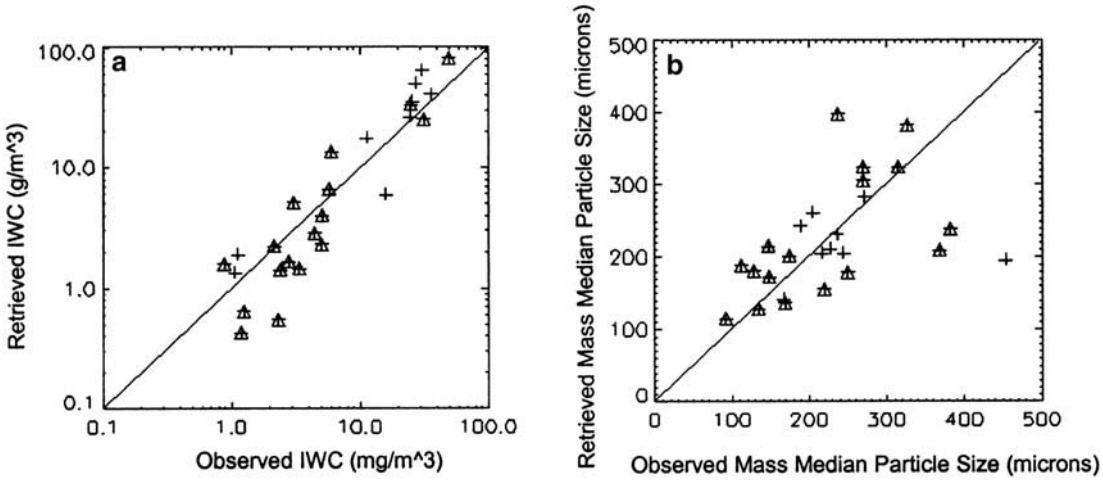

Figure 13. Comparison of retrieved (abscissa) to aircraft-observed (ordinate) cirrus microphysical properties. In Figure 13a, IWC is plotted, and in Figure 13b, mass median particle size is plotted. The symbols with triangles indicate those comparisons where the observed and derived radar reflectivity matched to within 2 dB.

Many of the observations in the larger size ranges have correspondingly large radar reflectivity and warm temperatures. According to the analysis presented earlier, we expect many of these distributions to be significantly bimodal or otherwise not well characterized by an exponential function. However, we have made no attempt here to screen the aircraft data for observations with significant bimodality.

4.2. Statistical Comparison With In Situ Data

[40] An intensive observing period was held during March 2000 at the SGP ARM site whose purpose was to observe the local three-dimensional cloud structure with multiple mm radars and in situ aircraft (UND Citation). The UND Citation was instrumented with a full suite of PMS probes during the IOP including the 2DC and 2DP so that the full spectrum of cirrus particles important to radar remote sensing could be faithfully sampled. Additionally, the Citation carried the counter flow virtual impactor (CVI; *Twohy et al.* [1997]) to measure the *IWC* directly as well as the Cloud Particle Imager (CPI; *Lawson et al.* [2001]) to observe the habit distribution of cirrus crystals. To assist in this IOP, the NOAA Environmental Technology Laboratory scanning Ka band cloud radar (NOAA-K; *Kropfli et al.* [1995]) was stationed at the SGP Central Facility. The NOAA-K operates in the same frequency band as the MMCR and was situated approximately 700 m from the MMCR during the observing period. Our goal here is to use the scanning data collected by the NOAA-K combined with the MMCR to alleviate the sample volume problems typical of aircraft-ground base cloud property comparisons.

[41] On 9 March a cirrus system was intensively sampled over the ARM site by the ground and airborne instruments. Figure 5 shows the height-time cross section of Doppler moments observed by the MMCR during the cirrus event. We have already discussed the 9 March case above. Additional information concerning the in situ data and the case in general is also given by *Heymsfield and Iaquinta* [2000] and *Heymsfield et al.* [2002]. The Citation began collecting data along 75 km level legs centered on the CART site near cloud top (9.4 km) at approximately 19:20 UTC. During the ensuing 90 minutes, the Citation conducted 5 level legs, stepping down through the cloud layer during the period. Table 7 lists the details of the legs and the designations we will use when referring to them.

[42] The NOAA-K radar collected data using a scan pattern during this event designed to observe the three-dimensional structure of the cloud layer as it advected and

Table 6. Comparison of Retrieved IWC and L_{MM} to That Observed by Aircraft During Overpasses of the MMCR During the Flights Listed in Table 1[a]

	dB*Z* Difference Less Than 5 dB	dB*Z* Difference Less Than 2 dB	dB*Z* Difference Less Than 0.5 dB
IWC r	0.93	0.95	0.97
IWC Med Error	0.58	0.57	0.52
$L_{MM}r$	0.47	0.50	0.66
L_{MM} Med Error	0.32	0.30	0.27

[a]*IWC r* and $L_{MM}r$ denote the correlation coefficient and *IWC* Med Error and L_{MM} Med Error denote the fractional median error of the *IWC* and L_{MM}. The columns denote differences between the MMCR-observed Z_e and that derived from aircraft particle spectra.

Table 7. Level Leg Parameters of 9 March 2000 of the UND Citation Near the SGP ARM Site[a]

	Start-End, UTC	Height, km	NOAA-K Ze Mean, dB	ACFT Ze Mean, dB	NOAA-K Ze SDV, dB	ACFT Ze SDV, dB
Leg 1	19:19–19:41	9.4	−16.9	−18.6	4.4	3.4
Leg 2	19:48–20:04	8.5	−18.0	−19.5	4.4	3.9
Leg 3	20:05–20:17	8.3	−15.8	−19.5	4.7	3.6
Leg 4	20:18–20:32	8.0	−14.7	−19.4	5.2	3.8
Leg 5	20:33–20:57	7.7	−17.5	−19.9	3.9	3.4

[a]See Figure 5 for a graphical representation. Also shown are Z_e values observed along the flight track by the scanning NOAA-K radar and Z_e values calculated from the observed aircraft particle spectra. Figure 16 shows the histograms from which the Z_e statistics were compiled.

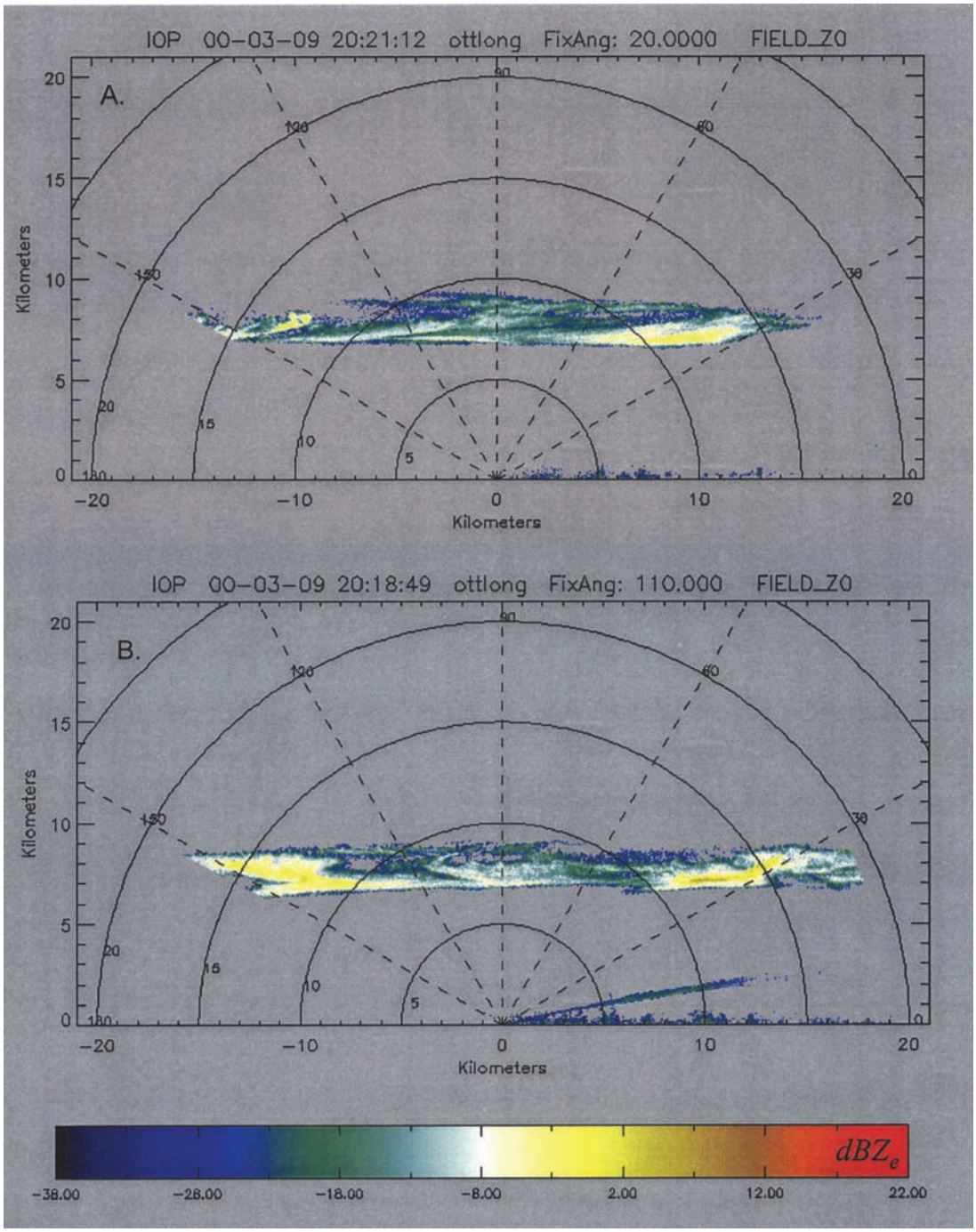

Figure 14. Radar reflectivity factor (dB*Ze*) collected by the NOAA-K scanning radar at the SGP ARM site on 9 March 2000. In Figure 14a the scan was approximately along the wind while in Figure 14b the scan was approximately across the wind at cirrus levels. These scans were collected during leg 4 (Table 5) of the UND Citation flight. Figure courtesy of NOAA ETL.

evolved overhead. The scan pattern consisted of consecutive over-the-top RHI scans along azimuths spaced 45 degrees apart in a clockwise manner. Each scan took approximately 1 minute and data were recorded as 3 second averages in 60 m range gates out to a range of 20 km. No effort was made to coordinate the scans of the NOAA-K with the in situ aircraft. The MMCR ran in the standard mode of operations during this case; data consist of approximately 10-second averages every 34 seconds, and the range gate spacing is 90m [*Clothiaux et al.*, 1999]. As an example, a NOAA-K reflectivity RHI scan is shown in Figure 14. This scan was conducted during leg 3 of the aircraft flight and is roughly oriented along the flight track the Citation was following (parallel to the local wind direction).

[43] Our approach to comparing the aircraft observations and the cloud properties retrieved from the MMCR data is reasonably straightforward and follows essentially from the techniques outlined by *Matrosov et al.* [1998] and earlier

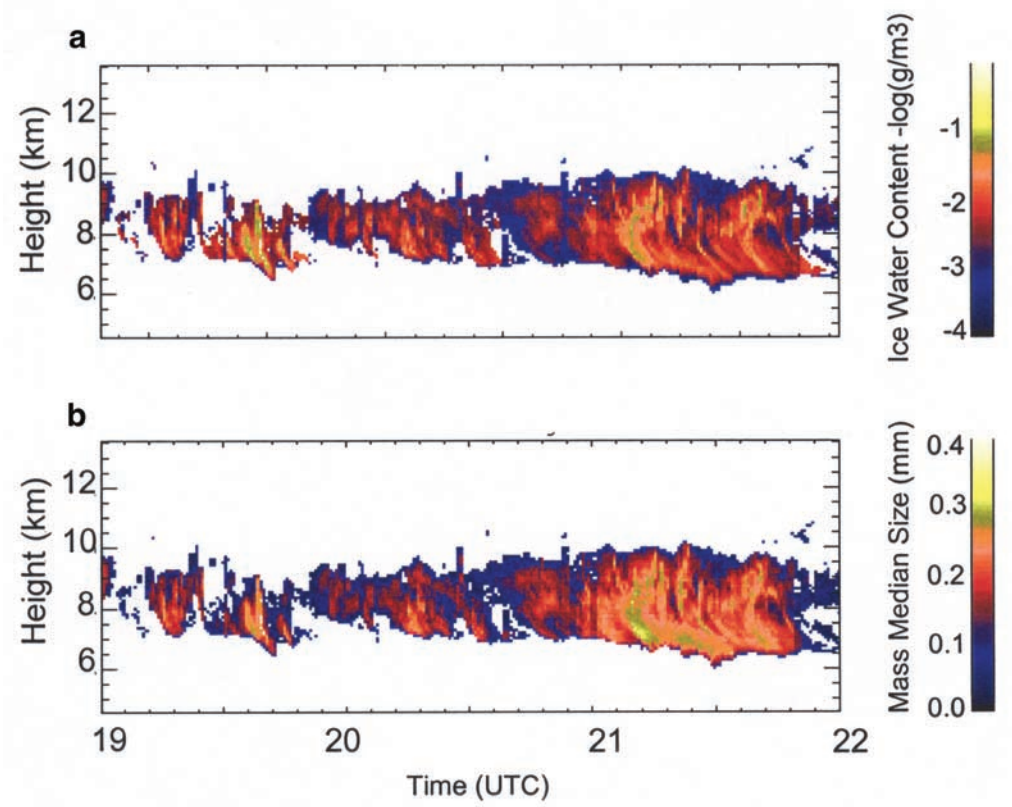

Figure 15. Microphysical parameters (a) IWC and (b) mass median particle size retrieved using the Doppler moments cloud property retrieval algorithm on 9 March 2000 at the SGP ARM site. Particle habits assumed were bullet rosettes. The input data are plotted in Figures 5a and 5d.

work published by *Heymsfield and Palmer* [1986]. The retrieval algorithm is operated normally using as input the data shown in Figure 5. The retrieved microphysical properties are shown in Figure 15. Regression relationships are then derived relating the derived *IWC* to the MMCR-observed Z_e assuming a power law relationship ($IWC = 0.103 Z_e^{0.516}$, where *IWC* is in g m^{-3}), and the retrieved L_{MM} to the MMCR-observed dBZ_e assuming a linear relationship ($L_{mm} = 339.0 + 7.1\ dBZ_e$, where L_{mm} is in μm). Applying these relationships to the NOAA-K radar reflectivity collected during a specified aircraft leg along the flight track and within 200m of the flight altitude is used to generate histograms of Z_e, *IWC* and L_{MM}. These histograms and their associated statistics are then compared directly to similar histograms derived from the *in situ* observations. With this technique, uncertainties about the sample volume are minimized since the aircraft and radar sampled the same general volume for many minutes. Figure 16 shows the results of this exercise for the five level legs listed in Table 8.

[44] The results, shown in Figure 16 and Table 8, are reasonably encouraging and in line with expectations. We find that for legs 1, 2, and 5, the Z_e histograms are reasonably similar (within 2.5 dBZ_e) suggesting a good match between the aircraft and radar sample volumes. Legs 3 and 4, on the other hand show a bias with the NOAA-K Z_e biased toward larger values. In general, the *IWC* histograms follow the Z_e results with legs 1 and 2 showing the best agreement and leg 3 and 4 biased high. This *IWC* difference is most significant for leg 4 where we find a difference in mean *IWC* of nearly a factor of two between the aircraft and radar. Particle size tends to show a somewhat better level of agreement with the histograms not quite so obviously biased. We do find that the particle size variance is consistently larger in the aircraft data compared to the radar. This discrepancy in variance is not seen in either the reflectivity or the IWC comparisons. Overall, the differences we find are consistent with the theoretical levels of uncertainty that we derived earlier.

5. Algorithm Implementation

[45] Finally, we would like to discuss implementation of the algorithm in an operational setting. This will also allow us to present a comparison of results from the algorithm described in this paper (hereinafter referred to as the Z-V algorithm) with similar results from another cloud property retrieval algorithm [*Mace et al.*, 1998b, 2001] (hereinafter referred to as the Z-R algorithm) that uses Z_e observations from the MMCR and downwelling radiance observations from the atmospheric emittance radiance interferometer (AERI). The Z-V algorithm contains several assumptions and empirical relationships that, in an operational environment may or may not be applicable for a given cirrus cloud system. We have attempted to address these sources of uncertainty throughout this work. The algorithm accuracy is quite dependent on the result of the implementation of the OK99 algorithm that results in an approximate separation of particle motions from air motion contributions to the Dop-

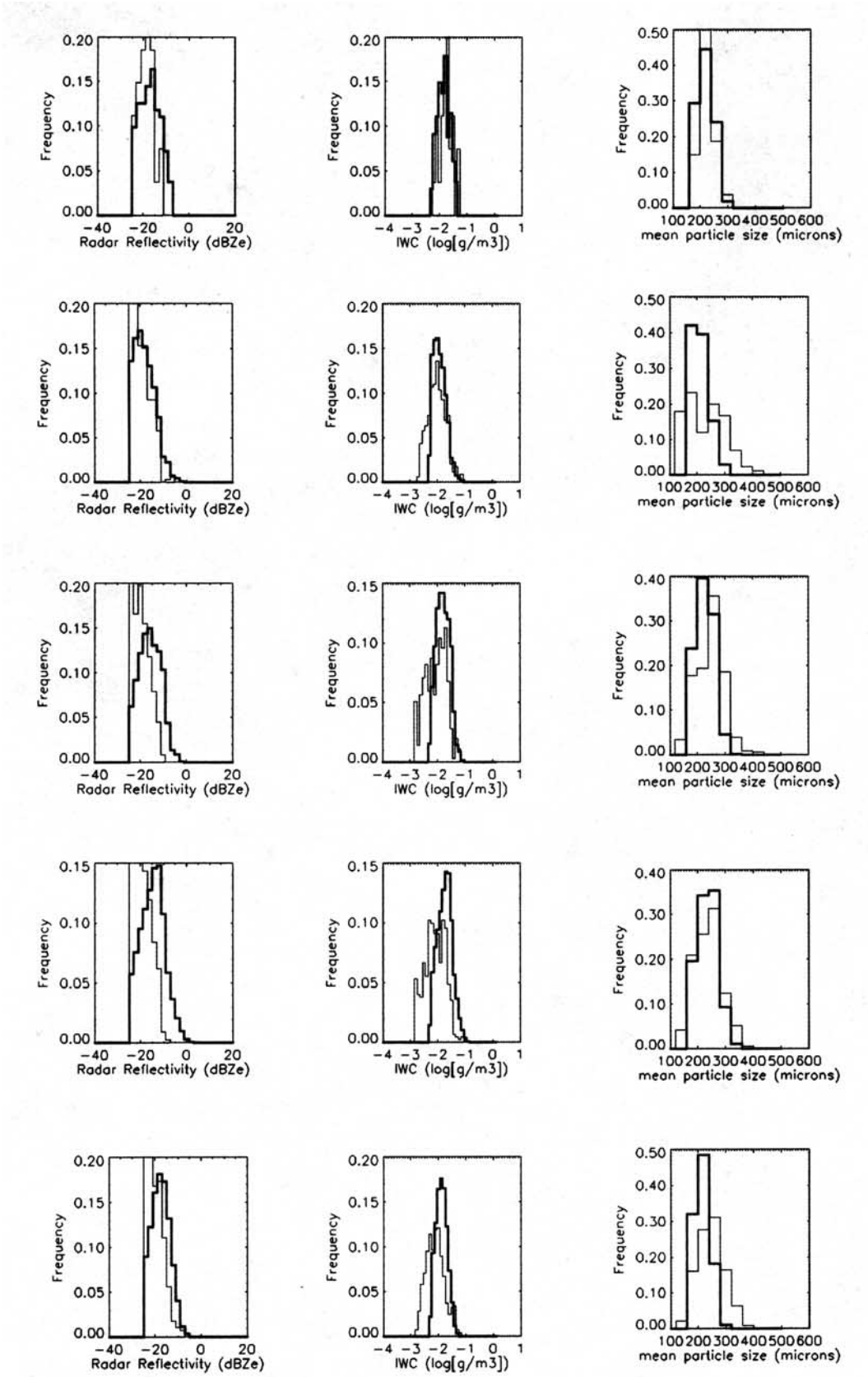

Figure 16. Comparison of cloud properties derived along the aircraft legs (Table 5) to cloud properties derived using the scanning NOAA-K radar and the vertically pointing MMCR. See text for details. Each row of plots corresponds to a flight leg (leg 1 is at the top, and 5 is at the bottom), and each column corresponds to a comparison quantity as indicated. The histogram shown with a thick line corresponds to parameters derived from radar data.

Table 8. Comparison of Microphysical Parameters Observed by the UND Citation and Derived From the Reflectivity Observations of the NOAA-K Cloud Radar[a]

	NOAA-K *IWC* Mean, g m^{-3}	ACFT *IWC* Mean, g m^{-3}	NOAA-K *IWC* SDV, g m^{-3}	ACFT *IWC* SDV, g m^{-3}	NOAA-K L_{MM} Mean, μm	ACFT L_{MM} Mean, μm	NOAA-K L_{MM} SDV, μm	ACFT L_{MM} SDV, μm
Leg 1	0.016	0.020	0.009	0.011	219.	238	31.6	48.1
Leg 2	0.014	0.013	0.009	0.011	211	261	31.5	84.2
Leg 3	0.018	0.012	0.011	0.011	226	280	33.1	84.6
Leg 4	0.022	0.011	0.015	0.010	235	299	36.7	83.5
Leg 5	0.014	0.010	0.007	0.010	214	301	28.0	77.5

[a]See the text for additional information.

pler velocity. Only a single case study was presented that showed a 20% uncertainty in $\overline{V}_d^q$. An assumption that is implicit in the OK99 algorithm that is also critical to the retrieval algorithm is that the particle mass-fallspeed relationship that exists in quiet air is preserved in the final result. Of course this correlation must be present in the data to begin with. Since the *IWC* and radar reflectivity are directly proportional, this correlation will also be present in the Z_e-V_d data. Another way of stating this is that larger particles that fall faster have more mass and larger radar reflectivity than smaller particles. This would hold as well for an ensemble of particles. However, there are cases where the correlation between Z_e and V_d is dominated by fluctuating mean air motions where both the magnitude and the fluctuations of the air motions are large with respect to the increase in V_d with increasing mean particle size in the cirrus layer. In these cases, $\overline{V}_d^q$ cannot be expected to have sufficient accuracy or precision for use in the Z-V algorithm. These fluctuations can conceivably take place on any timescale reasonably important to the cirrus field under consideration to include a steady trend in the mesoscale vertical velocity during the event or rapid fluctuations associated with small-scale wave activity or turbulence. Our goal is to find a means of diagnosing these occurrences as best we can, and derive a simple set of criteria that will allow us to discriminate between cases when air motion fluctuations dominate the fallspeed-mass correlation.

[46] Our approach is to compile case by case statistics of comparisons between the Z-V results and the *Z*-R results under the assumption that the *Z*-R results, beyond the few aircraft cases we have examined, provides the best measure of the actual cloud properties. We then search for a relationship between the correlation coefficients of V_d with Z_e, T, and Δ (r_Z, r_T, and $r\Delta$) and the statistics of the correlation (R), slope of the linear regression line (m), and bias (b) derived by comparing the ice water path (*IWP*) and effective radius (r_{eff}) reported by the two algorithms in single cirrus events. Only those cases with at least 20 comparison points are used. Based on approximately 160 cirrus events observed over approximately 2.5 years, the results of this exercise are reported in Table 9. Interestingly, we find that the actual magnitude of r_Z has little bearing on the statistics of the goodness of the comparison. We should note also, that no cases with substantially negative correlation have been found; obviously such cases should be discarded. What does appear to be related to the goodness of the comparison is the relationship between r_Z and r_T or $r\Delta$. Table 9 shows that when $r_Z > 2r_T$, the comparison improves substantially compared to cases when $r_Z < r_T$, This result is reasonable when compared to Table 2b. Since under most circumstances, $\overline{V}_d^q$ is primarily determined by the relationship between Z_e and V_d, when Z_e and V_d are largely uncorrelated, the regression is mostly determined by T and Δ. T and Δ were meant to serve as second order corrections to the assumed relationship between Z_e and V_d. When the relationship between Z_e and V_d is absent or substantially weak, the algorithm performs poorly. While we will continue to develop these statistics and fine tune our understanding of the algorithm as we implement the procedure on the continuing MMCR data stream, for the time being we will consider a case not suitable for retrieval when $r_Z < 1.5\ r_T$. Using this criterion, approximately 40% of the cirrus cases considered in the 2.5-year period were not suitable for retrieval. This rate of rejection should be considered a significant limitation of the Z-V algorithm.

6. Summary

[47] With the advent of multiple continuously operating research facilities that include millimeter radars for cloud studies, it has become necessary to develop techniques to fill gaps in our current cloud property retrieval technology. While the current set of algorithms that use primarily radar reflectivity and downwelling radiance [*Matrosov et al.*, 1992, 1994; *Mace et al.*, 1998b] or alternatively lidar extinction measurements [*Intrieri et al.*, 1993; *Wang and Sassen*, 2002] appear to be able to characterize cirrus cloud properties, these algorithms are limited to situations where the cloud layer is optically thin and not obscured by underlying cloud layers. These criteria exclude a significant fraction of the cirrus that are observed by millimeter radar. Therefore, reasoning that the only information in addition to Z_e that are routinely available in conditions where the layer is optically thick or otherwise obscured by underlying clouds

Table 9. Correlation Coefficient *R*, Slope of the Linear Regression *m*, and Fractional Bias of IWP and r_{eff} From the Z-V and Z-R Algorithms[a]

	$r_Z < r_T$	$r_Z < 1.25\ r_T$	$r_Z > 1.75\ r_T$	$r_Z > 2\ r_T$
		R		
IWP	0.57	0.53	0.78	0.77
r_{eff}	0.61	0.66	0.79	0.78
		m		
IWP	0.71	1.1	1.2	1.1
r_{eff}	0.31	0.54	0.90	0.90
		Bias		
IWP	0.80	1.3	0.50	0.50
r_{eff}	0.80	0.46	0.44	0.50

[a]Values are listed in terms of the correlation ratios between $\overline{V}_d$ and Z_e and $\overline{V}_d$ and T.

are the first and second moments of the Doppler spectrum (Doppler velocity and spectrum width), we have explored the information content of these quantities in terms of development of algorithms for retrieving the microphysical properties of cirrus. The algorithm described in this paper is not designed in its current state as a replacement for the well-established multisensor approaches but as a supplement to what is currently available. Note also that *Matrosov et al.* [2002] have recently proposed an approach similar to that outlined here.

[48] In developing this technique, we first ascertained what degree of complexity is needed to capture the essential characteristics of cirrus particle size distributions by analyzing in situ data gathered during several flights of the UND Citation over the SGP ARM site. These data suggested that while bimodal size distributions are a frequent occurrence at warmer than average cirrus temperatures and at larger than average radar reflectivities for cirrus, the basic characteristics of the size distribution could be reasonably well characterized by unimodal functional approximations. Significant error is first encountered at radar reflectivites more than about -5 dBZ_e. We also established that two-parameter exponential functions are capable of modeling the characteristics of these size distributions to within the observational uncertainty of the PMS data. Error due to this simplifying assumption first becomes evident for cirrus with temperatures larger than about -20c where the distributions become bimodal and broaden significantly. As in situ probes become more reliable at measuring the smallest particles of the cirrus particle spectra, this issue should be reevaluated.

[49] The first and second Doppler moments are composed of contributions due to the Doppler velocity of the particles in quiet air modulated by the up and downdrafts that are occurring within the cloud. Since we do not have available the full Doppler spectrum, rigorous deconvolution of these two components are not possible. Therefore we are forced to adopt approximate techniques. Reasoning that the vertical motion magnitude is proportional to spatial scale and identifying approximate scale breaks that are more or less specified by the cloud event temporal scale and the scale of the radar sample volume, we assume that the largest scales of motion (those that are external to the cloud system) can be neglected. *Orr and Kropfli* [1999] generalized an approach first discussed and used by *Matrosov et al.* [1994] to treat air motions internal to the cloud event (those motions that lead to the majority of the variability in the mean Doppler velocity). They assume that volumes with similar characteristics have similar quiet air fallspeeds and that the air motions are sufficiently random so that they can be removed by averaging. We evaluated this technique with aircraft data and found uncertainties of approximately 20% in a particular case. Air motion variability internal to the sample volume of the radar tends to broaden the Doppler spectrum and is recorded in the Doppler spectrum width. We extended Orr and Kropfli's reasoning to $\bar{\sigma}_d$ and further assumed that since turbulence only broadens the spectrum, we searched for the least broad resolution volumes that had similar sets of characteristics and assumed that these values of spectrum width were applicable to other volumes with similar characteristics. Accuracy on the 40% level was found by applying this approach to synthetic Doppler moments derived from aircraft data. Since three-parameter functions are not necessarily required to meet our goals here, we do not use the second moment information directly in the retrieval algorithm except to exclude turbulent volumes in the OK99 regression algorithm. However, there may be applications that will allow for direct use of the second moment such as using the additional information provided by the second moment to construct an over determined system of equations that could then be solved in a least squares sense. With additional study and improved accuracy in observations, the second Doppler moment could also be used as the third equation in a retrieval algorithm built around fully determined gamma functions. We leave these items to future research.

[50] Having identified a set of simplifying assumptions and validated a data processing approach to use the Doppler moments, we applied a set of empirical relationships relating the radar backscatter cross section, the crystal terminal velocity and the crystal mass to the crystal maximum dimension, to develop an algorithm that relates the radar observations to associated microphysical properties. This approach was shown to be sensitive to the crystal habit that is assumed for the distribution. Using synthetic Doppler moments data perturbed realistically for observational error in a sensitivity study where the habit was varied randomly among several habits that are typical of cirrus, we determined that the algorithm uncertainty is roughly 60% for IWC and 40% for median particle size. This level of uncertainty was confirmed in comparisons of retrieval results to in situ data.

[51] While these results are satisfactory, clearly more work is needed. The sensitivity to particle habit and the related sensitivities to empirically derived mass- and fall-speed-dimensional relations limit the general application of the algorithm to situations where we are reasonably confident that the empirical results are valid. For instance, applying the power law relations listed in Table 3 designed for synoptically forced middle latitude cirrus to tropical cirrus may result in larger than expected uncertainties. It is critical, therefore, to increase our empirical base of information in other types of cirrus cloud systems such as tropical cirrus.

[52] **Acknowledgments.** Funding for this work was provided by the Environmental Science Division of the U.S. Department of Energy (grant DE-FG0398ER62571) and through a NASA EOS Validation Program grant (NAG56458). The research of AJH was partially supported by NASA/EOS (grant S-97894-F). The contributions of MP were supported by a U.S. Department of Energy grant DE-FG03-97ER62360 and Battelle Pacific Northwest National Laboratory contract 354794-AQ8. Data were obtained from the Atmospheric Radiation Measurement Program sponsored by the U.S. Department of Energy, Office of Science, Office of Biological and Environmental Research, Environmental Sciences Division. We appreciate the assistance of Shelby Frisch and the NOAA ETL team for providing the scanning radar data.

References

Ackerman, T. P., K. N. Liou, F. P. Valero, and L. Pfister, Heating rates in tropical anvils, *J. Atmos. Sci.*, *45*, 1606–1623, 1988.

Atlas, D., The estimation of cloud parameters by radar, *J. Meteorol.*, *2*, 309–317, 1954.

Atlas, D., Advances in radar meteorology, *Adv. Geophys.*, *10*, 317–478, 1964.

Atlas, D., and S. Bartnoff, Cloud visibility, radar reflectivity and drop size distribution, *J. Meteorol.*, *1*, 143–148, 1953.

Atlas, D., S. Y. Matrosov, A. J. Heymsfield, M.-D. Chou, and D. B. Wolff, Radar and radiation properties of ice clouds, *J. Appl. Meteorol.*, *34*, 2329–2345, 1995.

Aydin, K., and T. M. Walsh, Millimeter wave scattering from spatial and planar bullet rosettes, *IEEE Trans. Geosci. Remote Sens.*, *37*, 1138–1150, 1999.

Babb, D. M., J. Verlinde, and B. W. Rust, The removal of turbulent broadening in radar Doppler spectra using linear inversion with double-sided constraints, *J. Atmos. Oceanic Technol.*, *17*, 1583–1595, 2000.

Clothiaux, E. E., K. P. Moran, B. E. Martner, T. P. Ackerman, G. G. Mace, T. Uttal, J. H. Mather, M. A. Miller, and D. J. Rodriguez, The Atmospheric Radiation Measurement Program cloud radars: Operational modes, *J. Atmos. Oceanic Technol.*, *16*, 819–827, 1999.

Clothiaux, E. E., T. P. Ackerman, G. G. Mace, K. P. Moran, R. T. Marchand, M. A. Miller, and B. E. Martner, Objective determination of cloud heights and radar reflectivities using a combination of active remote sensors at the ARM CART sites, *J. Appl. Meteorol.*, *39*, 645–665, 2000.

Danne, O., M. Quante, D. Milferstadt, H. Lemke, and E. Raschke, Relationships between Doppler spectral moments within large-scale cirro- and altostratus cloud fields observed by a ground-based 95-GHz cloud radar, *J. Appl. Meteorol.*, *38*, 175–189, 1999.

Doviak, R. J., and S. S. Zrnic, *Doppler Radar and Weather Observations*, 562 pp., Academic, San Diego, Calif., 1993.

Ebert, E. E., and J. A. Curry, A parameterization of ice cloud optical properties for climate models, *J. Geophys Res.*, *97*, 3831–3836, 1992.

Frisch, A. S., C. W. Fairall, and J. B. Snider, Measurement of stratus cloud and drizzle parameters in ASTEX with Ka-band Doppler radar and microwave radiometer, *J. Atmos. Sci.*, *52*, 2788–2799, 1995.

Fu, Q., and K. N. Liou, Parameterization of the radiative properties of cirrus clouds, *J. Atmos. Sci.*, *50*, 2008–2025, 1993.

Gossard, E. E., Measurement of cloud droplet size spectra by Doppler radar, *J. Atmos. Oceanic Technol.*, *11*, 712–726, 1994.

Gu, Y., and K. N. Liou, Interactions of radiation, microphysics, and turbulence in the evolution of cirrus clouds, *J. Atmos. Sci.*, *57*, 2463–2479, 2000.

Gultepe, I., and D. O'C. Starr, Dynamical structure and turbulence in cirrus clouds: Aircraft observations during FIRE, *J. Atmos. Sci.*, *52*, 4159–4182, 1995.

Heymsfield, A. J., Cirrus uncinus generating cells and the evolution of cirriform clouds, part 2, Structure and circulations of the cirrus uncinus generating head, *J. Atmos. Sci.*, *32*, 809–819, 1975.

Heymsfield, A. J., Precipitation development in stratiform ice clouds, *J. Atmos. Sci.*, *34*, 367–381, 1977.

Heymsfield, A. J., and L. J. Donner, A scheme for parameterizing ice-cloud water content in general circulation models, *J. Atmos. Sci.*, *47*, 1865–1877, 1990.

Heymsfield, A. J., and J. Iaquinta, Cirrus crystal terminal velocities, *J. Atmos. Sci.*, *57*, 916–938, 2000.

Heymsfield, A. J., and A. G. Palmer, Relationships for deriving thunderstorm anvil ice mass for CCOPE storm water budget estimates, *J. Clim. Appl. Meteorol.*, *25*, 691–702, 1986.

Heymsfield, A. J., and J. L. Parrish, Computational technique for increasing the effective sampling volume of the PMS two-dimensional particle size spectrometer, *J. Appl. Meteorol.*, *17*, 1566–1572, 1978.

Heymsfield, A. J., and J. L. Parrish, Interactive system for processing PMS two-dimensional imaging probe data, *J. Atmos. Oceanic Technol.*, *3*, 724–739, 1986.

Heymsfield, A. J., and C. M. R. Platt, Parameterization of the particle size spectrum of ice clouds in terms of the ambient temperature and the ice water content, *J. Atmos. Sci.*, *41*, 846–855, 1984.

Heymsfield, A. J., and R. M. Sabin, Cirrus crystal nucleation by homogeneous freezing of solution droplets, *J. Atmos. Sci.*, *46*, 2252–2264, 1989.

Heymsfield, A. J., S. Lewis, A. Bansemer, J. Iaquinta, L. M. Miloshevich, M. Kajikawa, C. Twohy, and M. R. Poellot, A general approach for deriving the properties of cirrus and stratiform ice cloud particles, *J. Atmos. Sci.*, *59*, 3–29, 2002.

Hogan, R. J., and A. J. Illingworth, Deriving cloud overlap statistics from radar, *Q. J. R. Meteorol. Soc.*, *126*, 2903–2909, 2000.

Intrieri, J. M., G. L. Stephens, W. L. Eberhard, and T. Uttal, A method for determining cirrus cloud particle sizes using lidar and radar backscatter technique, *J. Appl. Meteorol.*, *32*, 1074–1082, 1993.

Jensen, E. E., O. B. Toon, L. Pfister, and H. B. Selkirk, Dehydration of the upper troposphere and lower stratosphere by subvisible cirrus clouds near the tropical tropopause, *Geophys. Res. Lett.*, *23*, 825–828, 1996.

Kosarev, A. L., and I. P. Mazin, An empirical model of the physical structure of upper layer clouds, *Atmos. Res.*, *26*, 213–228, 1991.

Kropfli, R. A., S. Y. Matrosov, T. Uttal, B. W. Orr, A. S. Frisch, K. A. Clark, B. W. Bartram, R. F. Reinking, J. B. Snider, and B. E. Martner, Cloud physics studies with 8 mm wavelength radar, *Atmos. Res.*, *35*, 299–313, 1995.

Larson, H., J.-F. Gayet, G. Febvre, H. Chepfer, and G. Brogniez, Measurement errors in cirrus cloud microphysical properties, *Ann. Geophys.*, *16*, 266–276, 1998.

Lawson, R. P., B. A. Baker, C. G. Schmitt, and T. L. Jensen, An overview of microphysical properties of Arctic clouds observed in May and July 1998 during FIRE ACE, *J. Geophys. Res.*, *106*, 14,989–15,014, 2001.

Lin, R.-F., A numerical study of the evolution of nocturnal cirrus by a two-dimensional model with explicit microphysics, Ph. D. dissertation, 198 pp., Pa. State Univ., State College, 1997.

Liu, C., and A. J. Illingworth, Toward more accurate retrievals of ice water content from radar measurements of clouds, *J. Appl. Meteorol.*, *39*, 1130–1146, 2000.

Lohmann, U., and E. Roeckner, Influence of cirrus cloud radiative forcing on climate and climate sensitivity in a general circulation model, *J. Geophys. Res.*, *100*, 16,306–16,323, 1995.

Mace, G. G., and S. Benson-Troth, Cloud layer overlap characteristics derived from long-term cloud radar data, *J. Clim.*, *15*, 2505–2525, 2002.

Mace, G. G., D. O'C. Starr, T. P. Ackerman, and P. Minnis, Examination of coupling between an upper tropospheric cloud system and synoptic scale dynamics diagnosed from wind profiler and radiosonde data, *J. Atmos. Sci.*, *52*, 4094–4127, 1995.

Mace, G. G., T. P. Ackerman, E. E. Clothiaux, and B. A. Albrecht, A study of composite cirrus morphology using data from a 94-GHz radar and correlations with temperature and large scale vertical motion, *J. Geophys. Res.*, *102*, 13,581–13,593, 1997.

Mace, G. G., C. Jakob, and K. P. Moran, Validation of hydrometeor prediction from the ECMWF model during winter season 1997 using millimeter wave radar data, *Geophys. Res. Lett.*, *25*, 1645–1648, 1998a.

Mace, G. G., T. P. Ackerman, P. Minnis, and D. F. Young, Cirrus layer microphysical properties derived from surface-based millimeter radar and infrared interferometer data, *J. Geophys. Res.*, *103*, 23,207–23,216, 1998b.

Mace, G. G., E. E. Clothiaux, and T. P. Ackerman, The composite characteristics of cirrus clouds: Bulk properties revealed by 1-year of continuous cloud radar data, *J. Clim.*, *14*, 2185–2203, 2001.

Matrosov, S. Y., and A. J. Heymsfield, Use of Doppler radar to assess ice cloud particle fall velocity-size relations for remote sensing and climate studies, *J. Geophys. Res.*, *105*, 22,427–22,436, 2000.

Matrosov, S. Y., T. Uttal, J. B. Snider, and R. A. Kropfli, Estimates of ice cloud paramters from ground-based infrared radiometer and radar measurements, *J. Geophys. Res.*, *97*, 11,567–11,574, 1992.

Matrosov, S. Y., B. W. Orr, R. A. Kropfli, and J. B. Snider, Retrieval of vertical profiles of cirrus cloud microphysical parameters from Doppler radar and infrared radiometer measurements, *J. Appl. Meteorol.*, *33*, 617–626, 1994.

Matrosov, S. Y., R. F. Reinking, R. A. Kropfli, and B. W. Bartram, Estimation of ice hydrometeor types and shapes from radar polarization measurements, *J. Atmos. Oceanic Technol.*, *13*, 85–96, 1996.

Matrosov, S. Y., A. J. Heymsfield, R. A. Kropfli, B. E. Martner, R. F. Reinking, J. B. Snider, P. Piionen, and E. W. Eloranta, Comparison of ice cloud parameters obtained by combined remote sensor retrievals and direct methods, *J. Atmos. Oceanic Technol.*, *15*, 184–196, 1998.

Matrosov, S. Y., A. Korolev, and A. J. Heymsfield, Profiling ice mass and characteristic particle size from Doppler radar measurements, *J. Atmos. Oceanic Technol.*, *19*, 1003–1018, 2002.

McFarquhar, G. M., A. J. Heymsfield, J. Spinhirne, and B. Hart, Thin and subvisual tropopause tropical cirrus: Observations and radiative impacts, *J. Atmos. Sci.*, *57*, 1841–1853, 2000.

Mitchell, D. L., Use of mass- and area-dimensional power laws for determining precipitation particle terminal velocities, *J. Atmos. Sci.*, *53*, 1710–1723, 1996.

Mitchell, D. L., S. K. Chai, Y. L. Liu, A. J. Heymsfield, and Y. Dong, Modeling cirrus clouds, part 1, Treatment of bimodal size spectra and case study analysis, *J. Atmos. Sci.*, *53*, 2952–2966, 1996.

Moran, K. P., B. E. Marner, M. J. Post, R. A. Kropfli, D. C. Welsh, and K. B. Widener, An unattended cloud-profiling radar for use in climate research, *Bull. Am. Meteorol. Soc.*, *79*, 443–455, 1998.

Orr, B. W., and R. A. Kropfli, A method for estimating particle fall velocities from vertically pointing Doppler radar, *J. Atmos. Oceanic Technol.*, *16*, 29–37, 1999.

Platt, C. M. R., Remote sounding of high clouds, part 1, Calculation of visible and infrared optical properties from lidar and radiometer measurements, *J. Appl. Meteorol.*, *18*, 1130–1143, 1979.

Platt, C. M. R., A parameterization of the visible extinction coefficient of ice clouds in terms of the ice/water content, *J. Atmos. Sci.*, *54*, 2083–2098, 1997.

Platt, C. M. R., and Harshvardan, Temperature dependence of cirrus extinction: Implications for climate feedback, *J. Geophys. Res.*, *93*, 11,051–11,058, 1988.

Platt, C. M. R., S. A. Young, P. J. Manson, G. R. Patterson, S. C. Marsden, R. T. Austin, and J. H. Churnside, The optical properties of equatorial cirrus from observations in the ARM pilot radiation observation experiment, *J. Atmos. Sci.*, *55*, 1977–1996, 1998.

Ramanathan, V., and W. Collins, Thermodynamic regulation of ocean warming by cirrus clouds deduced from observations of the 1987 El Nino, *Nature*, *351*, 27–32, 1991.

Randall, D. A., K.-M. Xu, R. J. C. Somerville, and S. Iacobellis, Single-column models and cloud ensemble models as links between observations and climate models, *J. Clim.*, *9*, 1683–1697, 1996.

Rashke, E., International Satellite Cloud Climatology Project, ISCCP, and its European Regional Experiment ICE (International Cirrus Project), *Atmos. Res.*, *21*, 191–201, 1988.

Rossow, W. B., and R. A. Schiffer, Advances in understanding clouds from ISCCP, *Bull. Am. Meteorol. Soc.*, *80*, 2261–2287, 1999.

Sassen, K., and G. C. Dodd, Homogeneous nucleation rate for highly supercooled cirrus cloud droplets, *J. Atmos. Sci.*, *45*, 1357–1369, 1988.

Sassen, K., D. O'C. Starr, and T. Uttal, Mesoscale and microscale structure of cirrus clouds: Three case studies, *J. Atmos. Sci.*, *46*, 371–381, 1989.

Sassen, K., J. M. Comstock, Z. Wang, and G. G. Mace, Clouds and aerosol research capabilities at FARS: The Facility for Atmospheric Remote Sensing, *Bull. Am. Meteorol. Soc.*, *82*, 1119–1138, 2001.

Sassen, K., D. O'C. Starr, G. G. Mace, P. Brown, Z. Wang, and M. Poellot, Midlatitude cirrus cloud derived from Hurricane Nora: A case study with implications for ice crystal nucleation and shape, *J. Atmos. Sci.*, in press, 2002.

Spinhirne, J. D., Micro pulse lidar, IEEE Trans, *Geosci. Remote Sens.*, *31*, 48–55, 1993.

Starr, D. O'C., Cirrus-cloud experiment: Intensive field observations planned for FIRE, *Bull. Am. Meteorol. Soc.*, *68*, 119–124, 1987.

Starr, D. O'C., and S. K. Cox, Cirrus clouds, part 1, Cirrus cloud model, *J. Atmos. Sci.*, *42*, 2663–2681, 1985.

Starr, D. O'C., and D. P. Wylie, The 27–28 October 1986 FIRE cirrus case study: Meteorology and clouds, *Mon. Weather Rev.*, *118*, 2259–2287, 1990.

Stephens, G. L., S.-C. Tsay, P. W. Stackhouse, and P. J. Flatau, The relevance of the microphysical and radiative properties of cirrus cloud to climate and climatic feedback, *J. Atmos. Sci.*, *47*, 1742–1753, 1990.

Stokes, G. M., and S. E. Schwartz, The Atmospheric Radiation Measurement (ARM) Program: Programmatic background and design of the cloud and radiation test bed, *Bull. Am. Meteorol. Soc.*, *75*, 1201–1221, 1994.

Twohy, C. H., A. J. Schanot, and W. A. Cooper, Measurement of condensed water content in liquid and ice clouds using an airborne counterflow virtual impactor, *J. Atmos. Oceanic Technol.*, *14*, 197–202, 1997.

Wang, Z., and K. Sassen, Cirrus cloud microphysical property retrieval using lidar and radar measurements, part 1, Algorithm description and comparison with in situ data, *J. Appl. Meteorol.*, *41*, 218–229, 2002.

A. J. Heymsfield, Meteorology Division, National Center for Atmospheric Research, P.O. Box 3000, Boulder, CO 80307, USA. (heyms1@ncar.ucar.edu)

G. G. Mace, Department of Meteorology, University of Utah, 819 Browning Building, 135 S. 1460 East, Salt Lake City, UT 84112, USA. (mace@met.utah.edu)

M. R. Poellot, Department of Atmospheric Sciences, University of North Dakota, P. O. Box 9006, Grand Forks, ND 58201, USA. (poellot@aero.und.edu)